Computation of Some Properties of Ti - Si -C and Ti - Al - N MAX Phase Materials

Vuyokazi Lusanda Bangani

A thesis submitted to the Faculty of Science,

University of the Witwatersrand,

in fulfillment of the requirement for the degree of

Masters of Science.

School of Physics,

University of the Witwatersrand,

Johannesburg,

South Africa.

May 5, 2010

Contents

List of Figures

List of Tables

Declaration

I declare that this dissertation is my unaided work and that all material contained therein has been duly acknowledged. It is being submitted for the degree of Masters of Science in the University of the Witwatersrand, Johannesburg. It has not been submitted before for any degree or examination in any University,

_____

(Signature of Candidate)

_____day of_____2010

To God and my parents

Publication Work

V. L. Bangani, J. E. Lowther "Electronic Structure and Relative Stabilities of the Ti-Al-N System" Elsevier (to be submitted)

Acknowledgements

Firstly I would like to thank God and my family for their support. Also I would like to thank my supervisor Professor J. E. Lowther for his supervision. My colleagues, Mahlaga Molepo and Kutemba Kapanji are acknowledged.

Finally I would like to thank the National Research Foundation / Department of Science and Technology, University of the Witwatersrand, Johannesburg , and the DST/NRF Center of Excellence in Strong Materials for financial support.

Abstract

The "MAX" phases are a class of ductile nanolaminated ternary nitrides and carbides, including about 60 known phases. The chemical formula for the MAX phase is $M_{n+1}AX_n$ where M is an early transition metal, A is for the A−group elements and X which can be either carbon (C) or nitrogen (N). They consists of the 211, 321 and 412 groups. There are over 40 M_2AX phases in existence. These include 11 different A−group elements and 9 different early transition metals. The M_2AC MAX phase category is divided into two subgroups, the V(B) and VI(B) transition metals. There are three M_3AX_2 *(*Ti_3SiC_2*,* Ti_3GeC_2 and Ti_3AlC_2*)* and one M_4AX_3 *(*Ti_4AlN_3). As for the 321 MAX- phases the chemical formula can be written as Ti_3AC_2, where A = Al, Si, Ge. This group comprises of *(*Ti_3SiC_2*,* Ti_3GeC_2 and Ti_3AlC_2*).* MAX phase properties are of more than two elements. They can be "*sliced or diced*" using a manual hacksaw. These materials are used in applications such as industrial robots, disc drives, electronics and MEMS devices. Raw materials to make these materials are abundant and inexpensive *(*the cost of Ti...is roughly equal to that of titanium powder, between $20 and $40 per kilogram*).* Like other materials, they are affected by

defects and kink bands. They all have similar crystal structures and bond properties.

Chapter 1

Introduction

1.1 Ultra - Hard Materials

1.1.1 Diamond

Ultra-hard materials are used in many applications from oil exploration tools or abrasives, precision instruments that have scratch-resistant coatings, to glasses for watch faces. Diamond is the hardest material known and synthetic diamond is used in the commercial industry. As a hard material it has short covalent bonds of carbon atoms, which contribute to its hardness. One of its weaknesses is that it is oxidized when cutting steel. Diamond is formed by sp^3-bonded carbon atoms with two face-centered cubic lattices shifted by a vector $(a/4, a/4, a/4)$. The lattice parameter $a = 3.56683\mathring{A}$, and the lattice symmetry is Td and has the same structure as silicon.

Compared to other materials diamond does maintain its stability when exposed

to many chemicals. It is relatively stable especially at temperatures of less than 600 ^{0}C, even though this temperature is dependent on the pressure and the environment. At temperature $T < 600$ ^{0}C, it reacts weakly with carbide-forming elements *(*Si, Ti, Zr, Hf, V, Nb, Ta, Cr, Mo, W, Fe, Co, Ni, Y, Al and certain other rare earth metals*)*. Diamond has an impurity content. Brown diamonds have an abundance of extended structural defects such as dislocations. Diamonds are easily cleaved along extended planar defects *(*predominantly along twins*)*. Striking polycrystalline CVD (chemical vapour deposition) diamond films with a hammer will result in easy cracking along the grain boundaries.

Diamond is extremely difficult to polish. It has the lowest coefficient of thermal expansion (0.8x10^{-6} K^{-1}) and the highest thermal conductivity at room temperature. It has an indirect bad gap value of 5.48 eV at 77 K and 5.47eV at 300K [4]. Like other materials it does contain defects, primary defects, vacancies (single vacancy, which is the most studied defect in diamond) and interstitial type defects They can be generated in different ways such as irradiation, heat or plastic deformation [4], [5].

1.1.2 MAX Phases

MAX phase is a new group of materials. These materials have a nanolaminar structure of "merging" $M_{n+1}X_n$layers [6]. These nanolaminated atom arrangements lead to a low shear modulus, a property that is critical for low friction materials. "MAX " denotes the chemical composition of these phases, which can generally be written

as $M_{n+1}AX_n$, $n = 1, ..., 3$ where M is an early transition metal, A an s_p element, and $X =$ carbon (C)or nitrogen (N) Crystallography shows them as compounds with layers of A atoms with a host lattice containing voids into which layers of binary carbide or nitride octahedra are inserted [7]. Their initial discoveries and determination was done by Nowonty *et al.*, during the 1960s [8]. As with transitional carbides, the max phases have high hardness and high melting points and excellent electrical conductivity making them very suitable for technological applications.

They are good thermal conductors. Though machinable some of them are elastically quite stiff and lightweight and their intrinsic brittleness makes them poor structural materials. However, they carry with them a combination of both metallic and ceramic properties [1] which is the result of the highly anisotropic hexagonal crystal structure. In these structures the early transition metal atoms and the carbon and or nitrogen atoms form an octahedral edge sharing building (MX) block interleaved by pure $A-$ element layers as shown in Figure (1.1). To date "MAX" phases materials form into three groups, based on the number of atoms of the M, A and X elements in each molecule and known as $211, 312$ and 413 phases with the stoichiometries M_2AX,M_3AX_2 and M_4AX_3 [8].

Max phases also have the rock salt structure. This structure consists of two interpenetrating *fcc* lattices, where each of the octahedral sites in either lattice is occupied by the other. The origin of the second fcc lattice is at an octahedral interstitial site of the first [9]. MAX carbides have improved ductility, oxidation

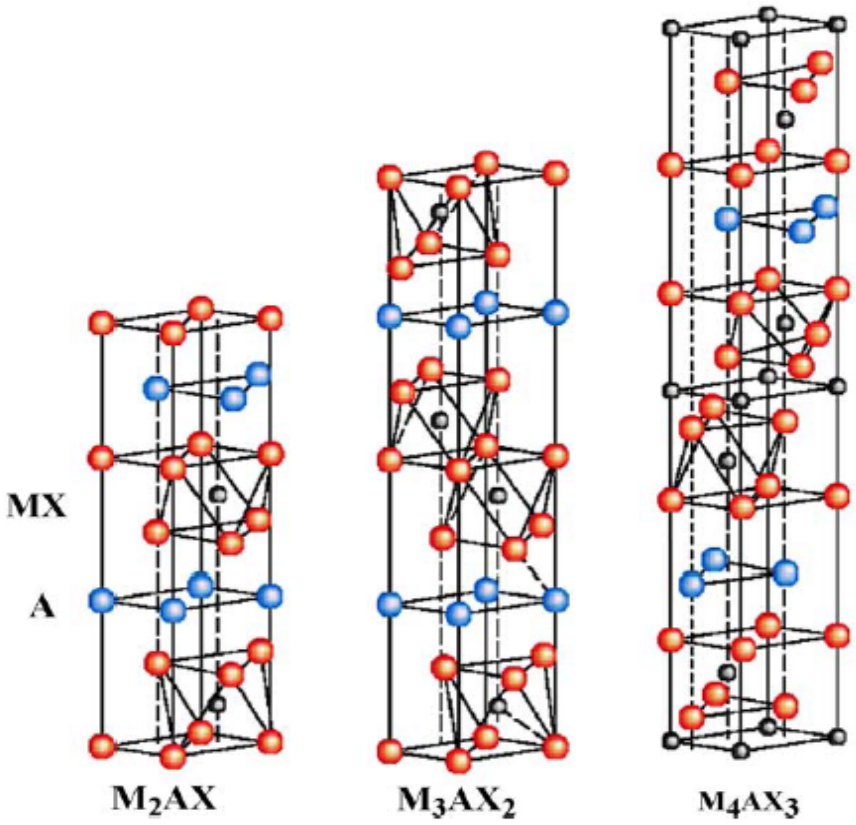

Figure 1.1: Hexagonal crystal for $M_{N+1}AXn$ phases (n = 1, ...,3) showing the different stacking in the existing subgroups of compositions M_2AX, M_3AX_2 and M_4AX_n. An early transition metal M *(red)*, an element from $A-$ groups usually $IIIA$ and IVA *(blue)* and third element X, which is either nitrogen or carbon *(black)*[1]

resistance and electrical conductivity. They have good damage tolerance and thermal shock resistance [1]. The M_2AC max phases, (where M =Ti,Zr,Hf,V,Ta,Cr,Mo, W asnd A = Al, Ga and Sn)with group IV elements, have significantly lower bulk moduli (B) than other max phases. This is attributed to a weaker $M-$ d orbital and C -p orbital bonding in these materials [10],[6].

Like other materials they are susceptible to kink bands. Kink bands form when layered materials are loaded parallel to the layers causing dislocations. These dislocations then move in opposite directions and eventually arrange themselves in walls, which define the kink boundaries [1]. The fundamental and crucial difference the kink bands that form in the max phases materials and those in other materials is that even after the initiation of damage, the ternary phases can still carry substantial loads. This is called "*damage tolerance*". This damage tolerance is built into the structure at the atomic level [1]. For these materials deformation mechanism is because of kink-band formation at room temperature. These kink-bands are more easily formed during indentations when the basal planes are parallel to the surface. The MAX phase are suitable materials for the study of dislocation dynamics and interactions of walls or pile-ups with grain boundaries, and other obstacles [11].

1.2 Dissertation Outline

This dissertation is arranged as follows. Chapter 2 outlines techniques and methodology, Chapters 3 and 4 cover the theoretical background and calculations carried out

using computational modelling techniques in particular density functional theory approaches om both Ti- Si C- and Ti- Al N max phases respectively. The last chapter, Chapter 5 is the conclusion. A bibliography of references appearing in this work ends the dissertation.

Chapter 2

Techniques and Methodology

2.1 Theoretical Background

Electronic structure theory dates back to the 1920s with quantum theory. It explained experiments concerning the microscopic world at atomic and molecular level through Schrödinger's wave equation. The Schrödinger equation forms the basis of almost every electronic structure calculation. Electronic structure calculations obtain the properties of a system from only the knowledge of the constituent atoms. The quantities which one would like to obtain by solving the Hamiltonian, and which are useful for the interpretation of experimental results, are related to both the ground state and the excited states of the many electron system. For example, calculation of the cohesive energy will require knowledge of ground state total energy, while the interpretation of a spectroscopic measurement will also require knowledge of excited

state energies. In these calculations the ground state geometry of many electron system is found by considering the change in the energy of the system with regard to the change in the positions of the atomic nuclei.

2.2 Theoretical Calculations

The work presented in this thesis is theoretical studies. The theoretical treatment used employed *"ab initio"* calculations to predict the plane stabilities and study the density of states (DOS). Ab initio *(or first principle)* calculation mean that the theory doesn't include any experimental data besides the structure. The theory is based on the interaction of charges (electron density). This approach is known as the Density Functional Theory (DFT) . For this work the Vienna Ab Initio Simulation Package ($VASP$) code was used. The VASP calculations were based on the local density approximation (LDA) , generalized gradient approximation approximation (GGA) and the plane - wave pseudo - potential to describe the electron density within crystal. The VASP method is known to be a fast computational method that gives accurate and reliable results. The DFT calculations output gave the total energy of the phase or structure. As of the formation energy, it was obtained from the difference of the calculated energy and the energy of the elements. The energy difference (ΔE) between the two phases structures were used to predict the relative stability. The 69 k- point mesh was used for all the calculations.

2.3 Vienna Ab Initio Simulation Package(VASP)

To solve the Schrödinger equation we have used the VASP Code. This is a package for performing ab-initio quantum-mechanical molecular dynamics (MD) using pseudopotentials and a plane wave basis set. Numerical simulations on VASP program, use the density functional theory with plane augmented wave (PAW) pseudopotentials [12]. Density functionals used are the generalized gradient approximation (GGA) to density functional theory using VASP code [10].

2.3.1 Density Functional Theory (DFT)

Density Functional Theory calculations are among the most frequently used theoretical tools in condensed matter physics. Density Functional Theory (DFT) is the theory of the electron structure of atoms, molecules and solids in their ground states in which the electronic density distribution $n(r)$ plays the central role which could also be applied to the many-electron wavefunction, $\Psi\left(r_1\sigma_{1.....}r_N\sigma_N\right)$ as a function of many variables [13].

The history of DFT was initiated by Thomas and Fermi in the 1920's by approximating the distribution of electrons in an atom. Thomas (1927) stated the following assumptions, *"Electrons are distributed uniformly in the six-dimensional phase space for the motion of an electron at the rate of two for each (h^3) of volume,"* and that there is an effective potential field that *"is itself determined by the nuclear charge and this distribution of electrons"*. These assumptions are viewed as the basis for the

derivation of the Thomas-Fermi formula for electron density [14].

DFT can be implemented via the Hohenberg-Kohn(HK) equation and the Kohn-Sham (KS) Theory. The Hohenberg-Kohn (HK) equation deals with the ground states of the electron structure especially in relation to the particle density and the Kohn-Sham Theory operates on the wave functions especially on single-particle orbitals [15]. The Hohenberg - Kohn - Sham Density Functional Theory (HKS-DFT) is based on the Shrödinger Theory. Based on the first theorem of Hohenberg- Kohn, the ground state wave function $\Psi_0 = \Psi[n_0]$ is the functional of the exact ground - state electronic density $\Psi(r)$, so that the expectation value of any observable is a unique function of the density. The wave function, Ψ_0,calculated from the Schrödinger equation for a single electron moving in a potential $v(r)$ is,

$$\left[-\frac{\hbar^2\nabla^2}{2m} + v(\mathbf{r})\right]\Psi_0 = \in \Psi_0 \tag{2.1}$$

and for more than one electron, the Schrödinger equation becomes

$$\left[\sum_i^N \left(-\frac{\hbar^2\nabla_i^2}{2m} + v(\mathbf{r}_i)\right) + \sum_{i<\mathrm{j}} U(\mathbf{r}_i,\mathbf{r}_j)\right]\Psi(\mathbf{r}_1,\mathbf{r}_{2.....},\mathbf{r}_N) = E\Psi((\mathbf{r}_1,\mathbf{r}_{2.....},\mathbf{r}_N) \tag{2.2}$$

where N is the number of electrons, and $U(\mathbf{r}_i,\mathbf{r}_j)$ the electron - electron interaction. The ground - state density does determine not only the ground - state wave

function Ψ_0,but also the potential $v(\mathbf{r})$;

$$v(\mathbf{r}) = v[n_0](\mathbf{r}) \tag{2.3}$$

and ground - state energy (E) given by:

$$(E_{v,0}) = E_v[n_o] = \left\langle \Psi[n_o] \left| \hat{H} \right| \Psi[n_o] \right\rangle \tag{2.4}$$

where $\hat{H} = \hat{T} + \hat{U} + \hat{V}$, has a variation property, and for a Coulomb system

$$\hat{U} = \sum_{i<\mathrm{j}} U(\mathbf{r}_i, \mathbf{r}_j) = \sum_{i<\mathrm{j}} \frac{q^2}{|r_i - r_j|} \tag{2.5}$$

and

$$\hat{T} = \frac{-\hbar^2}{2m} \sum_i \nabla_i^2 \tag{2.6}$$

The kinetic and interaction energies of a nonrelativistic Coulomb system can be described by universal operators,

$$E_v[n] = T[n] + U[n] + V[n] \tag{2.7}$$

with $T[n]$ and $U[n]$ as universal functions, and the potential energy $V[n]$,

$$V[n] = \int d^3r \; n(\mathbf{r})\, v(\mathbf{r}) \tag{2.8}$$

Now n_0 , not only determines the ground - state but the complete Hamiltonian (the operators $\hat{T}$ and $\hat{U}$ are fixed) and all excited states,

$$\Psi_k(\mathbf{r}_1, \mathbf{r}_{2.\ldots\ldots\ldots\ldots}, r_{\mathbf{N}}) = \Psi_k[n_0] \tag{2.9}$$

The associated Shrödinger equation with the electron density $n(\mathbf{r})$, in an electronic system is defined as the number of electrons per unit volume in a given state. The formula in terms of Ψ is

$$n(\mathbf{r}) = N \int \cdots \int |\Psi(\mathbf{r}_1,\ \mathbf{r}_{2,\ldots\ldots\ldots\ldots}, \mathbf{r}_N)|^2 \, ds_1,\ ds_{2\ldots\ldots\ldots\ldots\ldots\ldots\ldots\ldots} dx_N \tag{2.10}$$

This is a non-negative simple function of three variables x, y and z, integrating to the total number of electrons [15]. The ground - state energy $E(n)$ is therefore such a functional. The density is the expectation of a Hermitian Operator. The basic assumption in the Kohn - Sham version of the theory is that," *there exists a model-system of non-interacting fermion possessing the true interacting Schrodinger and non-interacting Kohn-Sham system*" [15]. These systems therefore define an electron - interaction energy functional which represents correlations due to the Pauli exclu-

sion principle and Coulomb repulsion and these correlations contribute to the kinetic energy from the wave function of the model system. This system is a single Slater determinant of the solutions of the Kohn-Sham equation, the ground-state density $n(r)$ and therefore the energy $E(n)$ [15].

2.3.2 The Hohenberg - Kohn Theorem

This approach formulates DFT as an exact theory of many - body systems to any system of interacting particles in an external potential $V_{ext}(\mathbf{r})$, for hard electrons and fixed nuclei, where the Hamiltonian can be written as

$$\hat{H} = -\frac{\hbar^2}{2m_e}\sum_i \nabla_i^2 + \sum_i V_{ext}(\mathbf{r}_i) + \frac{1}{2}\sum_{i\neq j}\frac{e^2}{|\mathbf{r}_i - \mathbf{r}_j|} \tag{2.11}$$

In Hartree atomic units $\hbar = m_e = e = 4\pi/\epsilon_0 = 1$.

The first theorem, **Theorem(1)** states that," *for any system of interacting particles in an external potential* $V_{ext}(\mathbf{r})$, *the potential* $V_{ext}(\mathbf{r})$ *is determined uniquely, except for a constant, by the ground state particle density* $n_0(\mathbf{r})$". **Theorem (2),** states that, "*A universal functional for the energy* $E[n]$ *in terms of the density* $n(r)$ *can be defined, valid for any external potential* $V_{ext}(\mathbf{r})$" [15].

The density of particles is pivotal in electron structure theory and its given by the

expectation value of the density operator $\hat{n}(\mathbf{r}) = \sum_i^N N\ \delta(\mathbf{r} - \mathbf{r}_i)$,

$$n(\mathbf{r}) = \frac{\langle \Psi \left| \hat{n}(\mathbf{r}) \right| \Psi \rangle}{\langle \Psi | \Psi \rangle} = N \frac{\int d^3r_2 ..... d^3r_N \sum_{\sigma 1} \sigma 1 \left| \Psi \left(\mathbf{r}_1, \mathbf{r}_2, \mathbf{r}_3, ..., \mathbf{r}_N \right) \right|^2}{\int d^3r_1 d^3r_2 .... d^3r_N \left| \Psi \left(r^1, r^2, r^3, ..., r_N \right) \right|^2} \tag{2.12}$$

As for the total energy of the expectation value of the Hamiltonian, in terms of $n(\mathbf{r})$, is

$$E = \frac{\left\langle \Psi \left| \hat{H} \right| \Psi \right\rangle}{\langle \Psi | \Psi \rangle} \equiv \left\langle \hat{H} \right\rangle = \left\langle \hat{T} \right\rangle + \left\langle \hat{V}_{int} \right\rangle + \int d^3r V_{ext}(\mathbf{r}) n(\mathbf{r}) + E_{11} \tag{2.13}$$

The kinetic energy operator for the electrons $\hat{T}$ is,

$$\hat{T} = \sum_i -\frac{1}{2} \nabla_i^2, \tag{2.14}$$

and $\hat{V}_{ext}$ the potential acting on the electrons due to the nuclei,

$$\hat{V}_{ext} = \sum_{i,1} V_1(|\mathbf{r}_i - \mathbf{R}_1|), \tag{2.15}$$

and $\hat{V}_{int}$ is the electron - electron interaction,

$$\hat{V}_{int} = \frac{1}{2} \sum_{i \neq j} \frac{1}{|\mathbf{r}_i - \mathbf{r}_j|} \tag{2.16}$$

The final term E_{11} is the electrostatic nucleus - nucleus *(or ion - ion)* interaction.

For any particular $V_{ext}(\mathbf{r})$, the exact ground state energy of the system is the global minimum value of this functional, and the density $n(\mathbf{r})$ minimizes the functional of the exact ground state density $n_0(\mathbf{r})$.

To prove the first theorem two different potentials $V_{ext}^{(1)}(\mathbf{r})$ and $V_{ext}^{(2)}(\mathbf{r})$ which differ by more than a constant but lead to the same ground state density $n(\mathbf{r})$ and two external potentials leading to two different Hamiltonians, $\hat{H}^{(1)}$ and $\hat{H}^{(2)}$ with different ground states wavefunctions, $\Psi^{(1)}$ and $\Psi^{(2)}$,this time assumed to have the same ground state density $n_0(\mathbf{r})$, are used to find the different $\Psi's$ with the same density. For $\Psi^{(2)}$ which is not the ground state of $\hat{H}^{(1)}$, therefore

$$E^{(1)} = \left\langle \Psi^{(1)} \left| \hat{H}^{(1)} \right| \Psi^{(1)} \right\rangle < \left\langle \Psi^{(2)} \left| \hat{H}^{(1)} \right| \Psi^{(2)} \right\rangle \tag{2.17}$$

Now considering the Hohenberg and Kohn arguments, the inequalities are if the ground state is non - degenerate. The last term can be written as

$$\left\langle \Psi^{(2)} \left| \hat{H}^{(1)} \right| \Psi^{(2)} \right\rangle = \left\langle \Psi^{(2)} \left| \hat{H}^{(2)} \right| \Psi^{(2)} \right\rangle + \left\langle \Psi^{(2)} \left| \hat{H}^{(1)} - \hat{H}^{(2)} \right| \Psi^{(2)} \right\rangle \tag{2.18}$$

$$= E^{(2)} + \int d^3r \left[V_{ext}^{(1)}(\mathbf{r}) - V_{ext}^{(2)}(\mathbf{r}) \right] n_0(\mathbf{r}), \tag{2.19}$$

so that

$$E^{(1)} < E^{(2)} + \int d^3r \left[V_{ext}^{(1)}(\mathbf{r}) - V_{ext}^{(2)}(\mathbf{r}) \right] n_0(\mathbf{r}). \tag{2.20}$$

For $E^{(2)}$, using the same way, the equation will be the same except for interchanged superscripts (1) and (2)

$$E^{(2)} < E^{(1)} + \int d^3r \left[V_{ext}^{(2)}(\mathbf{r}) - V_{ext}^{(1)}(\mathbf{r})\right] n_0(\mathbf{r}) \tag{2.21}$$

However, addition of equations (2.19) and (2.20), gives the contradictory inequality $E^{(1)}+ E^{(2)} < E^{(1)} + E^{(2)})$. This shows that there cannot be two different external potentials differing by more than a constant which gives rise to the same non- degenerate ground state. To prove **Theorem (2)**, the functional of the density, restricted space densities and also the restricted density of the ground state $n(\mathbf{r})$ electrons of the Hamiltonian with external potential V_{ext} in the Hohenberg - Kohn proof have to clearly defined. These $V-$ representatives make possible the construction of functionals of the density. If $n(\mathbf{r})$ is specified, each property is taken as a functional of $n(\mathbf{r})$. This includes the functional of $n(\mathbf{r})$ and the total energy functional,

$$E_{HK}[n] = T[n] + E_{int}[n] + \int d^3r V_{ext}(\mathbf{r}) n(\mathbf{r}) + E_{11} \tag{2.22}$$

$$\equiv F_{HK}[n] + \int d^3r V_{ext}(\mathbf{r}) n(\mathbf{r}) + E_{11} \tag{2.23}$$

where, E_{11} is the interaction energy of the nuclei [16].

2.3.3 Kohn-Sham Equations

This approach replaces the interacting many- body system in Hamiltonian with a different auxiliary system with an easier solution. In other words it " *replaces the many- body problem by an auxiliary independent - particle problem*" [16]. Moreover it has led to approximations that are presently the basis for most calculation attempts to make "*ab initio*" predictions for the properties of condensed matter and large molecular systems. To the interacting many-body problem, this approach rewrites the Hohenberg - Kohn expression for the ground state energy functional equation (2.22), in the form

$$E_{KS} = Ts\left[n\right] + \int d\mathbf{r}\ V_{ext}(\mathbf{r})n(\mathbf{r}) + E_{\text{Hatree}}\left[n\right] + E_{11} + E_{xc}\left[n\right] \tag{2.24}$$

This gives the density of the auxiliary system in terms of the sums of squares of the orbitals for each spin as,

$$n(\mathbf{r}) = \sum_{\sigma} n(r,\sigma) = \sum_{\sigma}\sum_{i=1}^{N^{\sigma}} \left|\Psi_i^{\sigma}(\mathbf{r})\right|^2,$$

the independent - particle kinetic energy T_s is given by

$$T_s = -\frac{1}{2}\sum_{\sigma}\sum_{i=1}^{N^{\sigma}} \left\langle \Psi_i^{\sigma} \left| \nabla^2 \right| \Psi_i^{\sigma} \right\rangle$$

and the Coulomb interaction energy of the electron density $n(\mathbf{r})$ interacting with

itself is

$$E_{Hatree}[n] = \frac{1}{2}\int d^3r d^3r' \frac{n\ (\mathbf{r})\, n\ (\mathbf{r'})}{|\mathbf{r} - \mathbf{r'}|}$$

All many - body effects of exchange and correlation are grouped into the exchange - correlation energy. Equations (2.22), (2.24) and $E = E_{HK}[n,s] \equiv \acute{E}_{HK}[n], (n$ *denotes the functional of the density which depends upon both space* r *and spin* $\sigma,)$ defining E_{xc} in terms of Hohenberg - Kohn functional equation (2.23) [16] as,

$$E_{xc}[n] = F_{HK}[n] - (T_s[n] + E_{Hatree}[n]),$$

or as

$$E_{xc}[n] = \left\langle \hat{T} \right\rangle - T_s[n] + \left\langle \hat{V}_{int} \right\rangle - E_{Hatree}[n]$$

2.3.4 Local Density Approximation (LDA)

LDA and DFT are based on the Hohenberg and Kohn theorems. The first Kohn-Sham calculation was performed by Tong and Sham (1966) by carrying out a comparison of the results between the calculated values of the Hartree-Fock and experiment [14]. The local density approximation (LDA) according to the Kohn -Sham calculations and the results of Laufer and Krieger (1986) [14], is by comparing the LDA and the exact solution in a soluble model of two interacting electrons in a quadratic external potential. On this case, the KS-LDA method gives accurate total energies but poor Kohn - Sham eigenvalues, based on the errors in the exchange-energy function.

Besides that the KS-LDA is also capable of describing molecular bonding, contrasting the non-bonding defect in the Thomas-Fermi Theory [14]. The (LDA) is then based mostly on the understanding of the non-interacting kinetic energy $\mathrm{T}_s[n]$ in the Thomas -Fermi Approximation.

$$T[n] \approx \int d^3r \; t^{\mathrm{hom}}(n \; (\mathbf{r})) \tag{2.25}$$

where $t^{\mathrm{hom}}(n)$ is the kinetic - energy density of a homogeneous interacting system with the density n, but for a non-interacting system the function t_s^{hom} for a single-particle is,

$$t_s^{\mathrm{hom}}(n) = \frac{3\hbar^2}{10m}\left(3\pi^2\right)^{\frac{2}{3}} n^{\frac{5}{3}} \tag{2.26}$$

where n is constant. But for an inhomogeneous system, with $n = n(\mathbf{r})$, one approximates

$$t_s(\mathbf{r}) \approx t_s^{\mathrm{hom}}(n \; (\mathbf{r})) = \frac{3\hbar^2}{10m}\left(3\pi^2\right)^{\frac{2}{3}} \int d^3 \; r \; n(\mathbf{r})^{\frac{5}{3}} \tag{2.27}$$

and obtains the full kinetic energy by integration over all space

$$\mathrm{T}_s^{LDA} \; [n] = \int d^3r \; t_s^{\mathrm{hom}}(n(\; \mathbf{r})) \tag{2.28}$$

$$= \frac{3\hbar^2}{10m}\left(3\pi^2\right)^{\frac{2}{3}} \int d^3r \int d^3 \; r \; n(\mathbf{r})^{\frac{5}{3}} \tag{2.29}$$

For the kinetic energy the approximation, $T_s[n] \approx T_s^{LDA}[n]$ in the Kohn-Sham

equations, but LDA is useful for another component of the total energy, the exchange-correlation energy $E_{xc}[n]$. For the exchange energy $E_x[n]$

$$e_x^{\text{hom}}(n) = -\frac{3q^2}{4}\left(\frac{3}{\pi}\right)^{\frac{1}{3}} n^{\frac{4}{3}} \tag{2.30}$$

so that

$$E_x^{LDA}[n] = -\frac{3q^2}{4}\left(\frac{3}{\pi}\right)^{\frac{1}{3}} \int d^3\, r\; n(\mathbf{r})^{\frac{4}{3}} \tag{2.31}$$

This is the local density approximation for the Thomas - Fermi Approximation [15].

2.3.5 Generalized Gradient Approximation (GGA)

The GGA calculations are performed for a wide variety of materials and is the method of choice for many first principles studies of materials and is comparative to LDA. Better GGA functionals are being developed because of the following reasons,

1) They improve the ground state properties of light atoms and molecules, clusters and solids composed of them;

2) They improve the many properties of 3d transition metals;

3) It over-corrects the LDA errors in lattice parameters [17]

The derivation of the second-order gradient expansion for the correlation energy in the high- density limit, numerically leads to the improperly positive correlation in energies for atoms because of the large size of the positive gradient size term. This led

to the proposal of the first generalized gradient approximation (GGA). Atoms show the second-order gradient approximation [14].

Further numerical tests of the gradient expansions for atoms show that the second-order gradient terms provide a useful correction to the Thomas -Fermi or local density approximation T_s and a helpful correction to the local density approximation for E_x [13]. The typical example of the correction to the Thomas-Fermi approximation of $T_s\,[n]$ [13], is given by

$$T_s\,[n] \;\approx\; T_s^W\,[n] = T_s^{LDA}\,[n]\;\frac{\hbar^2}{8m}\int d^3r\;\frac{\left|\nabla n\;(\mathbf{r})\right|^2}{n\,(\mathbf{r})} \tag{2.32}$$

The 2nd term on the right - hand side is the Weizsacker term with the lowest - order gradient correction and it never improves on the local density approximation (LDA).

$$E_x\,[n] \;\approx\; E_x^{GEA(2)}\,[n] \;=\; E_x^{LDA}\;[n] \;-\; \frac{10q^2}{432\pi\,(3\pi^2)^{\frac{1}{3}}}\int d^3r\;\frac{\left|\nabla n\,(\mathbf{r})\right|^2}{n\,(\mathbf{r})^{\frac{4}{3}}} \tag{2.33}$$

In more general functions of $n\,(\mathbf{r})$ and $\nabla_n\;\;(\mathbf{r})$, the generalized gradient approximation is of the form

$$E_{xc}^{GGA}\,[n] \;=\; \int d^3r\;f\,(n\,(\mathbf{r})\,,\nabla_n\;\;(\mathbf{r})) \tag{2.34}$$

Generalized gradient approximations (GGA's) for the exchange-correlation energy contributes in the improvement the local spin density (LSD) of atoms, molecules, and solids. The exchange-correlation energy $E_{xc} = E_x + E_C$ as a functional of the electron

spin densities $n_{\uparrow}$(r)and $n_{\downarrow}$(r) must be approximated. For this work we have employed the Perdew-Wang 1991 (PW91) functional as is an analytic fit to the numerical GGA. This is because the PW91 is capable of integrating some inhomogeneity effects while retaining many of the best features of LSD [18]. Now deriving the GGA correlation function in the form of

$$E_c^{GGA} = [n_{\uparrow}, n_{\downarrow}] = \int d^3 r n \left[\epsilon_c^{unif}(r_s, \zeta) + H(r_s, \zeta, t)\right] \tag{2.35}$$

where r_s is the local Seitz radius (n $=\frac{3}{4}\pi r_s = k_F^3/3\pi^2$), $\zeta = (n_{\uparrow} - n_{\downarrow})/n$ is the relative spin polarization and $t = \frac{|\nabla n|}{2\phi k_s n}$ is a dimensionless density gradient. Also to note is that $\phi(\zeta) = \left[(1+\zeta)^{\frac{2}{3}} + (1-\zeta)^{\frac{2}{3}}\right]/2$ is a spin-scaling factor and $k_s = (4k_F/\pi a_0)^{\frac{1}{2}}$ is the Thomas Fermi screening wave number with ($a_0 = \frac{\hbar^2}{me^2}$). In order to construct the gradient contribution H , three conditions have to be satisfied,

$$a)\ H \rightarrow (e^2/a_0)\beta\phi^3 t^2 \ldots\ldots\ldots\ldots\ldots\ldots\ldots\ldots\ldots \tag{2.36}$$

This is H as a second-order gradient expansion and limit t $\rightarrow 0$ and $\beta \simeq 0.066725$.

$$b)\ H\ \rightarrow -\epsilon_c^{unif} \ldots\ldots\ldots\ldots\ldots\ldots\ldots\ldots\ldots\ldots \tag{2.37}$$

As the limit t $\rightarrow \infty$, the sum rule on the correlation hole density gets satisfied as it equals to zero. The uniform scaling to the high-density limit and the correlation

energy must scale to a constant. H must cancel the logarithmic singularity of e_c^{unif} in the limit: $e_c^{unif}(r_s,\zeta) \rightarrow (e^2/a_0)\phi^3\left[\gamma \ln (r_s/a_0) - w\right]$ where w and γ are weak functions of ζ.*So*,

$$c)\ H \rightarrow (e^2/a_0)\gamma\phi^3 \ln t^2 \tag{2.38}$$

with $\gamma = (1\text{- } \ln 2)/\pi^2$. However, conditions a) ,b) and c) can be easily satisfied by

$$H = (e^2/a_0)\gamma\phi^3 x \ln\left\{1 + \frac{\beta}{\gamma}t^2\left[\frac{1+At^2}{1+At^2+A^2t^4}\right]\right\} \tag{2.39}$$

where $A = \frac{\beta}{\gamma}\left[\exp\{-\epsilon_c^{unif}/(\gamma\phi^3 e^2/a_0)\} - 1\right]^{-1}$. H appears as one of two terms in the PW91 correlation energy with γ= 0.025. Under uniform scaling to the high density limit, E_c^{GGA} tends to

$$-\frac{e}{a_0}\int d^3r\ \gamma\ \phi^3 x\ \ln\ \left[1 + \frac{1}{\chi s^2/\phi^2 + (\chi s^2/\phi^2)^2}\right] n \tag{2.40}$$

with a dimensionless gradient density $s = |\nabla_n|/2k_F n = (r_s/a_0)^{\frac{1}{2}}\phi t/c$ and $c = (3\pi^2/16)^{\frac{1}{3}} \simeq$ 1.2277 and $\chi = (\frac{\beta}{\gamma})c^2\exp(-\frac{w}{\gamma}) = 0.721\ 61$. Four further conditions are necessary for the GGA exchange energy to be constructed.

d) Under the uniform density scaling described along with condition (c), E_x must scale like λ. Thus, for $\zeta = 0$ everywhere, we must have

$$E_x^{GGA} = \int d^3r\ n\ \epsilon_x^{unif}(n)F_x(s) \tag{2.41}$$

where ϵ_x^{unif} = -3e$^2 k_F/4\pi$.

e) The exchange energy obeys the spin-scaling relationship

$$E_x\left[n_\uparrow, n_\downarrow\right] = \left(E_x\left[2n_\uparrow\right] + E_x\left[2n_\downarrow\right]\right)/2 \tag{2.42}$$

f) For the linear response of the spin-unpolarized uniform electron gas, meaning the LSD is the excellent approximation for the small density variations around the uniform density. For this linear response to be recovered, $s \longrightarrow 0$

$$F_x(s) \longrightarrow 1 + \mu s^2 \tag{2.43}$$

with $\mu = \beta(\pi^2/3)$, but the effective gradient coefficient for exchange cancels that for correlation.

g) The Lieb - Oxford bound

$$\begin{aligned} E_x\left[n_\uparrow, n_\downarrow\right] &\geq E_{xc}\left[n_\uparrow, n_\downarrow\right] \\ &\geq -1.679e^2 \int d^3r \ \mathrm{n}^{\frac{4}{3}} \end{aligned} \tag{2.44}$$

will be satisfied if the spin-polarized enhancement factor F_x grows readily with s to a maximum value less than or equal to 2.273. A simple $F_x(s)$ satisfying equations 2.43 and 2.44 and is

$$F_x(s) = 1 + \kappa - \frac{\kappa}{(1 + \mu s^2/\kappa)} \tag{2.45}$$

where $\kappa = 0.804$. The nonlocality. of the new GGA, is shown by defining the enhancement factor F_{x_C} over local exchange

$$E_{xc}^{GGA}[n_\uparrow, n_\downarrow] = \int d^3r \; n \; \epsilon_x^{unif}(n) F_{xc}(r_s, \zeta, s) \tag{2.46}$$

The correct features of LSD are retained by the proposed GGA, combining them with the most energetically important features of gradient-corrected nonlocality. However, the less important though correct features of PW91 sacrificed are (1) the correct second-order gradient coefficients for E_X and E_C in the slowly varying limit, and (2) correct nonuniform scaling of E_x in limits where the reduced gradient s tends to ∞ [18]. So Perdew, Burke and Ernzerhof (PEB) for the GGA calculations was used. PBE GGA simplifies the PW91 problems by generating a simplified GGA for the exchange relations in which all the parameters are fundamental constants [18].

2.3.6 Equation of States (Birch -Murnaghan Equation)

The Murnaghan Equation of State was derived by Francis D.Murnaghan of John Hopkins University in 1944. He showed that when a solid has a certain equilibrium volume (V_0) and the energy is increasing as volume either increased or decreased, dependence of energy (E) on volume would be harmonic solid with

$$E \;=\; E_0 \;+\; \frac{1}{2} B_0 \, \frac{(V - V_0)^2}{V_0} \tag{2.47}$$

The bulk modulus is

$$B \;=\; -\,V\left(\frac{\partial P}{\partial V}\right)_{T} \tag{2.48}$$

therefore making the energy (E), to be

$$E \;=\; E_0 + B_0\left(V_0 - V + V\ln\left(\frac{V}{V_0}\right)\right) \tag{2.49}$$

When pressure (P) is considered with the Bulk Modulus (B)

$$P \;=\; -\left(\frac{\partial E}{\partial V}\right) \tag{2.50}$$

$$B \;=\; -V\left(\frac{\partial P}{\partial V}\right) \tag{2.51}$$

Experimentally, the bulk modulus pressure derivative,

$$B' \;=\; \left(\frac{\partial B}{\partial P}\right)_{T} \tag{2.52}$$

is found to change little pressure. Taking $B' = B'_0$ to be constant,then

$$B \;=\; B_0 + B'_o P \tag{2.53}$$

where B_0 is the value of B when $P = 0$. We may equate this with equation (2.51)

and rearrange as

$$\frac{dV}{V} = -\frac{dP}{B + B_0^{'} P} \tag{2.54}$$

Integrating that , we obtain

$$P(V) = \frac{B_0}{B_0^{'}} \left(\left(\frac{V_0}{V} \right)^{B_0^{'}} - 1 \right) \tag{2.55}$$

Or equivalently

$$V(P) = V_0 \left(1 + B_0^{'} \frac{P}{B_0} \right)^{-\frac{1}{B_0^{'}}} \tag{2.56}$$

substituting equation (2.55) into $E = E_0 - \int P dV$ results in the equation of state for energy

$$E(V) = E_0 + \frac{B_o V}{B_0^{'}} \left(\frac{\left(\frac{V_0}{V} \right)^{B_0^{'}}}{B_0^{'} - 1} + 1 \right) - \frac{B_0 V_0}{B_0^{'} - 1}$$

However, the third - order Birch - Murnaghan isothermal equation of state, published in 1947 by Francis Birch of Harvard, is given by

$$P(V) = \frac{3B_0}{2} \left[\left(\frac{V_0}{V} \right)^{\frac{7}{3}} - \left(\frac{V_0}{V} \right)^{\frac{5}{7}} \right] \left\{ 1 + \frac{3}{4\left(B_0^{'} - 4\right) \left[\left(\frac{V_0}{V} \right)^{\frac{2}{3}} - 1 \right]} \right\} \tag{2.57}$$

2.4 Monkhorst-Pack Grid

Intergrating the Blöchl wave vector functions in the Brillion Zone(BZ) or certain portions are implemented in the calculations carried out for the electronic structure. The Blöchl wave is a function of a particle *(or an electron)*. It is the product of a planewave envelope function and a periodic function $U_k(\mathbf{r})$, which has the same periodicity as the potential :

$$\psi_k(\mathbf{r}) = U_k(\mathbf{r}) \exp(i\mathbf{k} \bullet \mathbf{r}) \tag{2.58}$$

where $U_k(\mathbf{r})$ has the period of a crystal lattice with $U_k(\mathbf{r}) = u_k(\mathbf{r} + \mathbf{T})$ [19]. We consider the presence of a set of periodic functions that are orthonormal in a uniformly spaced set of special points in the Brillion Zone (BZ). There has to be a lattice with primitive translation vectors t_1,t_2,t_3.and each lattice is unique if the lattice points are integers R_1,R_2,R_3, as

$$R = R_1 t_1 + R_2 t_2 + R_3 t_3 \tag{2.59}$$

the primitive reciprocal - lattice vectors are given by

$$b_1 = \frac{2\pi}{v} t_2 \text{ x } t_3, \; b_2 = \frac{2\pi}{v} t_3 \text{ x } t_1, \; b_3 = \frac{2\pi}{v} t_1 \text{ x } t_2 \tag{2.60}$$

where ν is the unit cell volume, and $b_1 - b_3$ are the reciprocal lattice with a *BZ*

volume of $\frac{8\pi 3}{v}$. We now take q as an integer for special points in the set, and u_r to be

$$u_r = (2r - q - 1)/2q \quad (r = 1, 2, 3, ..., q) \tag{2.61}$$

We now use u_{rs} in equation (2.61) to define

$$k_{prs} = u_p b_1 + u_r b_2 + u_s b_3 \tag{2.62}$$

Then in the **BZ** q^3 has distinct points. Now we let $A_m(k)$ be the sum taken all on R vectors (*star*) related to the operations of point group and considering that $A_m(k)$ is symmetric under all point-group operations, then

$$A_m(k) = N_m^{-\frac{1}{2}} \sum_{|R|=C_m} e^{ik.R} \tag{2.63}$$

C_m starts with $C_1 = 0$, N_m - no. of members in the m^{th} star of R. Considering the quantity $S_{mn}(q)$ as

$$S_{mn}(q) = \frac{1}{q^3} \sum_{p,r,s=1} A_m^*(k_{prs}) A_n(k_{prs}) \tag{2.64}$$

When equation (2.63) is substituted for A_m and A_n, then $S_{mn}(q)$ reduces to

$$S_{mn}(q) = (N_m N_n)^{-1/2} \sum_{a=1}^{N_m} \sum_{b=1}^{N_n} \prod_{j=1}^{3} W_j^{ab}(q) \tag{2.65}$$

sum a and sum b are over the members in the stars m and n, respectively with

$$W_j^{ab}(q) = \frac{1}{q}\sum_{r=1}^{q} e^{(\pi i/q)(2r-q-1)(R_j^b - R_j^a)} \tag{2.66}$$

and W_j^{ab} assumes the values:

$$\begin{aligned} W_j^{ab}(q) &= \{1 \quad if && \left|R_j^b - R_j^a\right| = 0, 2q, 4q.... \\ \{(-1)^{q+1}.....if \ \left|R_j^b - R_j^a\right| &= q, 3q, 5q..... \\ &= 0 \qquad \text{otherwise} \end{aligned} \tag{2.67}$$

One should bare in mind that q, R_j^b and R_j^a are integers. Imposing the restriction

$$\left|R_j^a\right| < q/2, \ \left|R_j^b\right| < q/2, \qquad (j = 1, 2, 3), \tag{2.68}$$

followed by

$$W_j^{ab}(q) = \delta(R_j^a, R_j^b)$$

Therefore using equation (2.65),

$$S_{mn}(q) = \delta_{mn} \tag{2.69}$$

and functions $A_m(k)$ for which equation (2.68) satisfied are orthonormal on the discrete set of BZ points k_{prs}. Since the the number of distinct terms of equation

(2.64) can be reduced by the lattice point-group symmetry, therefore

$$S_{mn}(q) = \frac{1}{q^3} \sum_{j=1}^{P(q)} w_i A_m(k_j) A_n(k_j) \tag{2.70}$$

where $P(q)$ is the symmetry-dependent number of points k_j from the set of points (k_{prs}) in the irreducible wedge of the BZ. Grouping the identical terms in equation (2.64) as a result of point-group symmetry, the result is equation (2.70). Other terms include the weight associated with k_j that is w_j,which represents the ratio of the order of the entire point group to the order of the group of the wave vector at k_j [20].

2.5 Pseudopotentials

The pseudopotential approach came as a result of an invention by C.Herring of an orthogonalized plane wave method. Pseudopotentials were originally introduced to simplify electronic structure calculations by eliminating the need to include atomic core state and strong potentials responsible for binding them [21], [16]. Phillips and Antoncik and Kleinman [16] later introduced an effective potential imitating the Pauli – repulsion by core electrons but balancing the electrostatic attraction by the nucleus in solids. This replaced the orthogonality. However, Hamann, Schluter and Chiang in 1979, showed the construction of pseudopotentials such that they have similar scattering properties to that of an atom to first order in energy. There are various reasons for the introduction of pseudopotentials. Two of those reasons are

- Avoiding the explicit description of core electrons.
- Avoiding swift oscillations of the wavefunction near the nucleus.

However, though pseudopotentials are quite accurate for large systems, they don't guarantee the production of the same results as an all – electron calculation in a molecule or solid. The error sources can be divided into two classes; the energy transferability problems and charge transferability problems.

2.5.1 Norm –Conserving Pseudopotentials

The norm-conserving concept, was first used by Topp and Hopfield in empirical pseudopotentials and was incorporated into ionic potentials by Starkloff and Joannopoulos. Bachelet, Hamann and Schluter later refined this procedure by introducing the construction of the atomic pseudo-orbital that is is free from relying on core states [22], [21]. To better understand the meaning of "norm – conserving" one has to be familiar with a list of requirements that comprise a " good " ab initio pseudopotential given by Hamann, Schluter and Chiang,

- All – electron and pseudo valence eigenvalues concur for the chosen atomic reference configuration.
- All – electron and pseudo valence wavefunctions agree beyond a chosen radius (R_c).
- The logarithmic derivatives of the all – electron and pseudo wavefunctions agree (R_c).

• The integrated charge inside (R_c) for each wavefunction agrees (norm -conservation).

• The first energy derivative of the logarithmic derivatives of the all-electron and pseudo wavefunctions agrees at R_c, and therefore for all r$\geq R_c$.

"Norm – conservation" is the key step in making a pseudopotential accurate and transferable so that a pseudopotential constructed in one environment *(an atom)* is able to describe the valence properties in a different environment including atoms, ions, molecules and condensed matter. " Norm – conserving " pseudopotentials attain accuracy by sacrificing a certain degree of "smoothness" and the degree of smoothness of the the pseudofunction on the contrary leads to a large cutoff radius. However, accuracy and transferability leads to a small cutoff radius R_c and "hard" potentials and "soft " potentials so as to simplify the description of wavefunctions in terms of basis functions [16],[22], [21].

2.5.2 Ultrasoft - pseudopotential

The Phillips-Kleinman construction has paved a way in understanding pseudopotentials. Pseudopotentials can be determined from either first principles calculations optimized pseudopotentials or experimental pseudo-potentials even though there is no great difference between the two. Various approximations to be determined when using pseudopotentials include self-consistent - field approximation. This is whereby the electron interaction is replaced by the potential depending upon the states occupied by electrons. These states are dependent on the potential including the Hartree

potential [23]. All potentials have to be soft meaning there is an expansion of the valence pseudo -functions using few plane waves. Transferability is also important as the pseudopotential for a specific atomic configuration should accurately generate others assuring that the differences between the crystal potential and atomic potential are addressed [17],[24],[16]. This construction encompasses also the projector operator equation which can be substituted in the Schrodinger equation where both the pseudopotential and pseudo - wave function are represented and the true wave function is related to the pseudo wave function [23].

There are different views from the Phillips-Kleinman construction such as those of Vanderbilt and co-workers. In their approach, the pseudo-wavefunctions and electron wavefunctions outside the core radius r_c are equal but inside they are allowed to be soft especially for norm - conserving potentials. This gives out the reduction of the plane wave cutoff needed in calculations. However there has to be an augmented term at the core region for computation of the pseudo - charge density needs rather than computing $\sum \varphi * \varphi$. When there is relaxation in the norm conservation the resulting pseudopotentials become less transferable. Vanderbilt pseudopotentials are used for large scale calculations for which the cost generation pseudopotentials is negligible compared to the cost calculations. Energy is written as, [17],

$$E = \sum_{occ} < \varphi_j \mid T + V^{NL} \mid \varphi_j > + \int d^3\mathbf{r} V^L(\mathbf{r}) \rho(\mathbf{r}) + \frac{1}{2} \int d^3\mathbf{r} d^3\acute{r} \frac{\rho(\mathbf{r}) \rho(\acute{\mathbf{r}})}{\mid \mathbf{r} - \acute{\mathbf{r}} \mid} + E_{xc}[\rho] + E_{ii} \tag{2.71}$$

where T is the kinetic energy operator, V^L is the local component of the pseudopotential, V^{NL} is the non-local Vanderbilt pseudopotential, the φ_j are the pseudo-wavefunctions and other terms. For V^{NL} a non-local separable used is [17],

$$V^{NL} = \sum_{mn} D^{(0)}_{nm} \mid \beta_n >< \beta_m \mid \tag{2.72}$$

This is considering one atom and the pseudopotential is characterized by the function β_m, the coefficients $D^{(0)}_{nm}$ and local component $V^L(r)$. The β_m are represented in an angular expansion i.e. spherical harmonics multiplied by radial functions (*typically one or two are used for each lm combination).* The radial functions vanish outside r_c. The pseudo-charge density ρ is given by the square of the pseudo-wavefunctions plus an augmentation inside the spheres.

$$\rho(r) = \sum_{occ} \left[\varphi^*_j(\mathbf{r}) \varphi_j(\mathbf{r}) + \sum_{mn} Q_{nm}(\mathbf{r}) < \varphi_j \mid \beta_n >< \beta_m \mid \varphi_j > \right] \tag{2.73}$$

where the $Q_{nm}(\mathbf{r})$ are local functions determined during the generation of the pseudopotential. Applying the variational principle to equations (2.71) to (2.73), the

secular equation is

$$H \mid \varphi_j >= \varepsilon_j \mathbf{S} \mid \varphi_j >, \tag{2.74}$$

with

$$H = T + V_{xc}(\mathbf{r}) + V_H(\mathbf{r}) + V^L(\mathbf{r}) + \sum_{mn} D_{nm} \mid \beta_n >< \beta_m \mid, \tag{2.75}$$

and

$$S = \mathbf{1} + \sum_{mn} q_{nm} \mid \beta_n >< \beta_m \mid,$$

where $\mathbf{1}$ denotes the identity operator and

$$q_{nm} = \int_{\alpha} d^3\mathbf{r} Q_{nm}(\mathbf{r}) \tag{2.76}$$

with the integral over the sphere defined by r_c. The D_{nm} are the $D_{nm}^{(0)}$ with a screening term.

$$D_{nm} = D_{nm}^{(0)} + \int_{\alpha} d^3\mathbf{r} V(\mathbf{r}) Q_{nm}(\mathbf{r}) \tag{2.77}$$

where V denotes the local potential, given the local pseudopotential plus the exchange correlation and Hartree potentials. For the ultrasoft pseudopotential generation the Vanderbilt scheme starts with all - electron atomic calculations in some

reference configuration. The radial Schrodinger equation is then solved within r_c at each E_{lj}, yielding regular solutions $\varphi lmj(\mathbf{r}) = u_{lj}(r)\mathbf{Y}_{lm}(\widehat{\mathbf{r}})$. For each (lmj), a smooth pseudopotential wavefunction, $\phi_{lmj}(r) = u_{lj}(\widehat{r})\,\mathbf{Y}_{lm}(\widehat{r})$ is generated subject only to the constraint that it matches smoothly onto φ_{lmj} at r_c, V^L, that matches the all - electron potentials outside r_c is determined. Construction of the orbitals,

$$\mid \chi_{lmj} >= \left[E_{lj} - T - V^L(\mathbf{r})\right] \mid \phi_{lmj} \tag{2.78}$$

follows. Since ϕ and V^L are equal to φ and all - electron potential, respectively, outside r_c, and φ satisfies the Schrodinger equation at E_{lj}, χ is zero outside r_c. Now the $Q_{nm}(\mathbf{r})$ can be constructed, since we know that it must account for the difference between the true charge density and $\phi * \varphi$

$$Q_{nm}(\mathbf{r}) = \varphi_n^*(\mathbf{r})\,\varphi_m(\mathbf{r}) - \phi_n^*(\mathbf{r})\,\phi_m(\mathbf{r}) \tag{2.79}$$

where n and m run over the $\{lmj\}$. In practice, a smoothing may be applied to Q_{nm} for facilitating the use with plane wave representations of the charge density. If this is done the smoothing is constructed to preserve the moments of the original Q_{nm}. Similarly $\mid \beta n\rangle$,is constructed as

$$\mid \beta_n >= \sum_m \left(\mathbf{B}^{-1}\right)_{mn} \mid \chi_m >, \tag{2.80}$$

with $\mathbf{B}_{nm} =< \phi_n \mid \chi_m >$. Using the identity shown below, components, V^L and

D_{nm}, are determined,

$$\left[T + V + \sum_{nm} D_{nm} \mid \beta_n >< \beta_m \mid\right] \mid \phi_n >= \tag{2.81}$$

$$E_n \left[\mathbf{1} + \sum_{nm} qnm \mid \beta_n >< \beta_m \mid\right] \mid \phi_n >, \tag{2.82}$$

which holds if

$$D_{nm} = \mathbf{B}_{nm} + E_m q_{nm} \tag{2.83}$$

Finally, the D_{nm} are unscreened using equation (2.81) to determine the $D_{nm}^{(0)}$ and the Hartree and exchange correlation contributions are subtracted from V to obtain V^L. The great attribute of this pseudo-potential is that the self- consistent iterations proceed, the contribution of the augmenting charge inside the sphere changes along with the wavefunctions. This charge contributes to the potential used in the Kohn-Sham equations. The evolution of the augmenting charge and its contribution to the potential during the calculation allows relatively large values of r_c to be used in the Vanderbilt construction. This yields very soft pseudopotentials, without sacrificing the accuracy of the calculation [17].

2.5.3 Projector Augmented Wave

According to Kresse and Jourbet, the projector augmented wave (PAW) method, is the combination of pseudopotential and linearized augmented-plane wave, done by Blöchl in an attempt to develop ultrasoft-pseudopotential [25]. Blöchl uses the linear transformation from the auxiliary to the all true wave function and derives the PAW total energy functional in a consistent manner applying this transformation to the Kohn-Sham(KS) functional [26]. The PAW method can also be defined as the pseudopotential method , that adapts to the instantaneous electronic environment and the augmented wave method. This method introduces the energy and potential independent basis sets [26].

Transformation Theory

The transformation in the PAW method expands the pseudo (PS) wave functions into plane waves (*basis sets*). Denoting the one-particle wavefunctions as $|\Psi_n\rangle$ and the auxiliary wavefunctions as $|\widetilde{\Psi}_n\rangle$. The tilde shows the smooth auxiliary wavefunctions, n is for a one-particle state with a band index, a spin index and a k - point. Transformation from the pseudo to the physical wave functions is denoted by T.

$$|\Psi_n\rangle = T|\widetilde{\Psi}_n\rangle \tag{2.84}$$

The constrained density functional F *(parameterized function of the gradients and*

its gradients) in terms of the pseudo(PS) wavefunctions is

$$F\left[|\widetilde{\Psi}_n\rangle, \Lambda_{m,n}\right] = E\left[T\ |\widetilde{\Psi}_n\right] - \sum_{n,m}\left[\langle\widetilde{\Psi}_n\left|T^\dagger T\right|\widetilde{\Psi}_n\rangle - \delta n, m\right]\Lambda m, n \tag{2.85}$$

$\Lambda m, n$ is the Lagrange multipliers. Looking at the variational principle in terms of the pseudo (PS) wavefunctions yields [26]

$$T^\dagger H T|\widetilde{\Psi}_n\rangle = \left|T^\dagger T\right|\widetilde{\Psi}_n\rangle\epsilon_n \tag{2.86}$$

$\epsilon_n(one-particle\ energies)$ are the eigenvalues of $\Lambda m, n\frac{f_n+f_m 9}{2f_n f_m}$. Equation (2.86) is Shrödinger - like, the Hamilton operator has a different form, $\widetilde{H} = T^\dagger H T$, an overlap $\widetilde{O} = T^\dagger T$ occurs, and this results in smooth pseudo (PS) wavefunctions. Evaluating the physical properties, also leads to the evaluation expectation values of an operator A, which can be expressed in terms of a true or pseudo (PS) wavefunctions.

$$\langle A\rangle = \sum_n f_n\langle\Psi_n\left|A\right|\Psi_n\rangle = \sum_n f_n\langle\widetilde{\Psi}_n\left|T^\dagger A T\right|\widetilde{\Psi}_n\rangle \tag{2.87}$$

For (PS) wavefunctions presentation, the transformed operator used is $\widetilde{A} = T^\dagger A T$ $(pseudo\ operator)$ which only holds for the valence electrons. These (PS) wavefunctions are used in the construction of all - electron (AE) wavefunctions and the total energy functional providing the missing link between augmented wave methods and the pseudopotential method. The (PS) wavefunctions are the variational parameters

instead of the (AE) functions in the PAW method.

Transformation Operator

The operator T has to modify the smooth (PS) wavefunction in each atomic region. Writing the transformation as an identity plus a sum of atomic contributions S_R

$$T = 1 + \sum_R S_R \tag{2.88}$$

S_R adds the difference between (AE) and (PS) wavefunctions. S_R local terms are defined in terms of solution $|\phi i\rangle$ of the Schrodinger equation for the isolated atoms and which will serve as the basis set. The valence wavefunctions can expressed as superposition with unknown coefficients [25] .

So

$$\Psi(\mathbf{r}) = \sum_{i\epsilon R} \phi_i(\mathbf{r}) c_i \qquad \text{for } |\mathbf{r} - \mathbf{R}_R| < r_{c,R} \tag{2.89}$$

$i \epsilon R$ is for the partial waves belonging to site R. The operator T produces only wavefunctions that are orthogonal to the core electrons. Therefore the atomic partial waves $|\phi_i\rangle$ include the valence states that are orthogonal to the core wavefunctions of the atom. For each of the partial waves an pseudo partial wave $|\widetilde{\phi}_i\rangle$.is chosen.The identity

$$|\phi_i\rangle = (1 + S_R)|\widetilde{\phi}_i\rangle \qquad \text{for } i\epsilon R \tag{2.90}$$

$$S_R|\widetilde{\phi}_i\rangle = |\phi_i\rangle - \widetilde{\phi}_i\rangle$$

shows the contribution of S_R to the transformation operator. $1 + S_R$ will change the wavefunction locally, therefore the partial waves $|\phi_i\rangle$ and the pseudo counter parts $|\widetilde{\phi}_i\rangle$ are needed even though they are pairwise identical beyond a certain radius $r_{c,R}$

$$\phi_i(\mathbf{r}) = \widetilde{\phi}_i(\mathbf{r}) \qquad \text{for i } \epsilon \text{ R and } |\mathbf{r} - \mathbf{R}_R| > r_{c,R} \tag{2.91}$$

Now applying the transformation operator to an arbitrary pseudo wavefunction, requires the expansion of the pseudo wavefunction locally into the pseudo partial waves.

$$\widetilde{\Psi}(\mathbf{r}) = \sum_{i\epsilon R} \widetilde{\phi}_i(\mathbf{r}) c_i = \sum_{i\epsilon R} \widetilde{\phi}_i(\mathbf{r}) \langle \widetilde{p}_i | \widetilde{\Psi} \rangle \qquad \text{for } |\mathbf{r} - \mathbf{R}_R| < r_{c,R} \tag{2.92}$$

defining the projector functions $|p_i^*\rangle$which probes the local character of the pseudo wave function in the atomic region. Equation(2.92) is used to deriving

$$\sum_{i\epsilon R} |\widetilde{\phi}_i\rangle\langle\widetilde{p}_i| = 1, \qquad \text{valid within } \mathrm{r_{c,R}} \tag{2.93}$$

Identity equation (2.92) holds for any pseudo wavefunction $|\widetilde{\Psi}\rangle$ and can be ex-

panded into pseudo partial waves $|\widetilde{\phi}_i\rangle$, if

$$\langle \widetilde{p}_i | \widetilde{\phi}_j \rangle = \delta_{i,j} \qquad \text{for i ,j } \epsilon R \tag{2.94}$$

So combining equations (2.90) and (2.91), allows us to apply S_R to any pseudo wavefunction

$$S_R|\widetilde{\Psi}\rangle = \sum_{i\epsilon R} S_R|\widetilde{\phi}_i\rangle\langle\widetilde{p}_i|\widetilde{\Psi}\rangle = \sum_{i\epsilon R}\left(|\phi_i\rangle - |\widetilde{\phi}_i\rangle\right)\langle\widetilde{p}_i|\widetilde{\Psi}\rangle \tag{2.95}$$

Therefore the transformation operator is

$$T = 1 + \sum_i \left(|\phi_i\rangle - |\widetilde{\phi}_i\rangle\right)\langle\widetilde{p}_i| \tag{2.96}$$

with a sum running over all partial waves of all atoms. The true wave function can be expressed as

$$|\Psi\rangle = |\widetilde{\Psi}\rangle + \sum_i \left(|\phi_i\rangle - |\widetilde{\phi}_i\rangle\right)\langle\widetilde{p}_i|\widetilde{\Psi}\rangle = |\widetilde{\Psi}\rangle + \sum_R \left(|\Psi^1_R\rangle - |\widetilde{\Psi}^1_R\rangle\right) \tag{2.97}$$

with

$$|\Psi^1_R\rangle = \sum_{i\epsilon R} |\phi_i\rangle\langle\widetilde{p}_i|\widetilde{\Psi}\rangle \tag{2.98}$$

$$|\widetilde{\Psi}^1_R\rangle = \sum_{i\epsilon R} |\widetilde{\phi}_i\rangle\langle\widetilde{p}_i|\widetilde{\Psi} \wedge \wedge\rangle \tag{2.99}$$

Expectation Values

Pseudo (PS) wavefunctions or all- electron (AE)wavefunctions provide the expectation values. From equation (2.87) with the 1^{st} sum for valence states and the other sum over core states $|\phi_n^c\rangle$.

$$\begin{aligned} \langle A \rangle &= \sum_n f_n \langle \Psi_n |A| \Psi_n \rangle + \sum_{n+1}^{N_c} \langle \phi_n^c |A| \phi_n^c \rangle \\ &= \sum_n f_n \langle \widetilde{\Psi}_n \left| T^\dagger A T \right| \widetilde{\Psi}_n \rangle + \sum_{n+1}^{Nc} \langle \phi_n^c |A| \phi_n^c \rangle \end{aligned} \tag{2.100}$$

where f_n represents the occupations of the valence states and N_c is the number of core states. The matrix element for a wave function Ψ in equation (2.95), can be decomposed into individual contributions like so,

$$\begin{aligned} \langle \Psi|A|\Psi \rangle &= \langle \widetilde{\Psi} + \sum_R \left(\Psi_R^1 \rangle - \widetilde{\Psi}_R^1 \right) |A| \widetilde{\Psi} + \sum_{R'} \left(\Psi_{R'}^1 - \widetilde{\Psi}_{R'}^1 \right) \rangle \qquad (2.101) \\ &= \underbrace{\langle \widetilde{\Psi}|A|\widetilde{\Psi} \rangle + \sum_R \left(\langle \Psi_R^1 |A| \Psi_R^1 \rangle - \langle \widetilde{\Psi}_R^1 |A| \widetilde{\Psi}_R^1 \rangle \right)}_{(1)} \\ &\quad \underbrace{+ \sum_R \left(\langle \Psi_R^1 - \widetilde{\Psi}_R^1 |A| \widetilde{\Psi} - \widetilde{\Psi}_R^1 \rangle + \langle \widetilde{\Psi} - \widetilde{\Psi}_R^1 |A| \Psi_R^1 - \widetilde{\Psi}_R^1 \rangle \right)}_{(2)} \\ &\quad \underbrace{+ \sum_{R \neq R'} \langle \Psi_R^1 - \widetilde{\Psi}_R^1 |A| \Psi_{R'}^1 - \widetilde{\Psi}_{R'}^1 \rangle}_{(3)} \end{aligned}$$

The local operators in the 2^{nd} and 3^{rd} parts vanish as partial wave expansion is converged, also $\Psi_R^1 - \widetilde{\Psi}_R^1$vanishes when its beyond the augmentation region as the partial waves are identical above this region. In case of a converged partial

wave expansion $\widetilde{\Psi} - \widetilde{\Psi}^1_R$function vanishes on its augmentation region or $\Psi^1_R - \widetilde{\Psi}^1_R$and $\widetilde{\Psi} - \widetilde{\Psi}^1_R$both functions become nonzero if there is no region of space, but $\Psi^1_R - \widetilde{\Psi}^1_R$ functions are never nonzero. Therefore equation (2.101), can be used to define the expectation value in equation (2.100) as

$$\begin{aligned}
\langle A \rangle &= \sum_n f_n \left(\langle \widetilde{\Psi}_n | A | \widetilde{\Psi}_n \rangle + \langle \Psi^1_n | A | \Psi^1_n \rangle - \langle \widetilde{\Psi}^1_n | A | \widetilde{\Psi}^1_n \rangle \right) && (2.102) \\
&\quad + \sum_{n=1}^{Nc} \langle \phi^c_n \, | A | \, \phi^c_n \rangle && (2.103) \\
&= \sum_n f_n \langle \widetilde{\Psi}_n | A | \widetilde{\Psi}_n \rangle + \sum_{n=1}^{Nc} \langle \widetilde{\phi}^c_n \, | A | \, \widetilde{\phi}^c_n \rangle \\
&\quad + \sum_R \left(\sum_{i,j \epsilon R} D_{i,j} \langle \phi_j \, | A | \, \phi_i \rangle + \sum_{n \epsilon R}^{N_{c,R}} \langle \phi^c_n \, | A | \, \phi^c_n \rangle \right) \\
&\quad - \sum_R \left(\sum_{i,j \epsilon R} D_{i,j} \langle \widetilde{\phi}_j \, | A | \, \widetilde{\phi}_i \rangle + \sum_{n \epsilon R}^{N_{c,R}} \langle \widetilde{\phi}^c_n \, | A | \, \widetilde{\phi}^c_n \rangle \right)
\end{aligned}$$

where $D_{i,j}$ is the one- centre density matrix defined as

$$D_{i,j} = \sum_n f_n \langle \widetilde{\Psi}_n | \widetilde{p}_j \rangle \langle \widetilde{p}_i | \widetilde{\Psi}_n \rangle = \sum_n \langle \widetilde{p}_i | \widetilde{\Psi}_n \rangle | f_n | \langle \widetilde{\Psi}_n | \widetilde{p}_j \rangle \tag{2.104}$$

$|\widetilde{\phi}^c_n\rangle$ the auxiliary core states allow the core wavefunctions into the plane - wave part causing the integrations of partial wave contributions to cancel beyond r_c. But these partial waves are identical to the true core states in the tails, but with a smooth continuation inside the atomic sphere. This scheme leads the electron density to be

$$
\begin{aligned}
n(\mathbf{r}) &= \widetilde{n}(\mathbf{r}) + \sum_{n} \left(n_R^1(\mathbf{r}) - \widetilde{n}_R^1(\mathbf{r}) \right) \\
\widetilde{n}(\mathbf{r}) &= \sum_{n} f_n \widetilde{\Psi}_n(\mathbf{r}) \widetilde{\Psi}_n(\mathbf{r}) + \widetilde{n}_c
\end{aligned}
\tag{2.105}
$$

$$
\begin{aligned}
n_R^1(r) &= \sum_{i,j \epsilon R} D_{i,j} \widetilde{\phi}_j(\mathbf{r}) \phi_i(\mathbf{r}) + n_{c,R} \\
\widetilde{n}_R^1(r) &= \sum_{i,j \epsilon R} D_{i,j} \widetilde{\phi}_j(\mathbf{r}) \widetilde{\phi}_i(\mathbf{r}) + \widetilde{n}_{c,R}
\end{aligned}
\tag{2.106}
$$

with $n_{c,R}$, the core density of the corresponding atom $\widetilde{n}_{c,R}$ being the identical and smooth pseudo core density outside the atomic region. There are instances whereby the matrix element of the general operator may be converging slowly with the converging plane- wave expression. This is because of *operator A* such as the singular electrostatic potentials of the nucleus. To avoid such problems from occurring, "intelligent zero" is added. Localized *operator B* at atomic region is used for pseudo wavefunction and the partial wave expansion as shown below and more importantly the addition of *operator B* improves the converged result. Not only that but *operator B* cancels out the problematic *operator A*.

$$
0 = \langle \widetilde{\Psi}_n \left| B \right| \widetilde{\Psi}_n \rangle \tag{2.107}
$$

2.5.4 Total Energy

The total energy expression is given by

$$E = \sum_n f_n \langle \Psi_n \left| -\frac{1}{2}\nabla^2 \right| \Psi n\rangle + \frac{1}{2}\int dr \int dr' \frac{\left(n+n^Z\right)\left(n+n^Z\right)}{|r-r'|} \quad (2.108)$$

$$+ \int dr n \epsilon_{xc}(n) \quad (2.109)$$

n^Z denoting the point charge density of the nucleus, ϵ_{xc}- is the energy per electron from exchange and correlation. Using the Hatree atomic units ($\hbar = e = m_e = 1$).

The contributors to E are

$$\widetilde{E} = \sum_n f_n \left\langle \Psi_n \left| -\frac{1}{2}\nabla^2 \right| \widetilde{\Psi_n} \right\rangle + \frac{1}{2}\int dr \int dr' \frac{\widetilde{n}+n'}{|r-r'|} \quad (2.110)$$

$$+ \int dr \widetilde{n} v + \int dr \widetilde{n} \epsilon_{xc}(\widetilde{n})$$

$$E^1 = \sum_{n,(i,j)} f_n \langle \widetilde{\Psi}_n | \widetilde{p}_i \rangle \langle \phi_i \left| -\frac{1}{2}\nabla^2 \right| \phi_j \rangle \langle \widetilde{p}_j | \widetilde{\Psi}_n \rangle \quad (2.111)$$

$$+ \frac{1}{2}\int dr \int dr' \frac{(n+n^Z)(n^1+n^Z)}{|r-r'|} + \int dr n^1 \epsilon_{xc}(n^1), \quad (2.112)$$

$$\widetilde{E^1} = \sum_{n,(i,j)} f_n \langle \widetilde{\Psi}_n | \widetilde{p}_i \rangle \langle \widetilde{\phi}_i | - \frac{1}{2}\nabla^2 | \widetilde{\phi}_j \rangle \langle \widetilde{p}_j | \widetilde{\Psi}_n \rangle \quad (2.113)$$

$$+ \frac{1}{2}\int dr \int dr' \frac{\left(\widetilde{n}^1+n'\right)\left(\widetilde{n}^1+n'\right)}{|r-r'|} + \int dr \widetilde{n}^1 \overline{v} + \int dr \widetilde{n}^1 \epsilon_{xc}(\widetilde{n}^1) \quad (2.114)$$

n -is the soft pseudo-charge density from the pseudo-wave functions on a plane-wave.

Then above equations are the contributors to E as E can be divided into $E = \widetilde{E} + E^1 - \widetilde{E}$. Potential $\overline{v}$, is used to minimize the truncation error, when the partial wave function isn't complete, but to the total energy it vanishes because of the onsite charge densities, $n^1 - \widetilde{n}^1$ in the augmented region. Rewriting the electrostatic energy E :

$$\frac{1}{2}\int dr \int dr' \frac{(\widetilde{n}+n')\,(\widetilde{n}+n')}{|r-r'|} = \frac{1}{2}\int dr \int dr' \frac{(\widetilde{n}+n')}{|r-r'|} + \int dr\ \widetilde{n}(\mathbf{r})v'(\mathbf{r}) + \sum_{R,R'} U_{R,R'} \tag{2.115}$$

The first term is for the smooth functions and evaluating it using the Fourier space becomes,

$$2\pi V \sum_{G} \frac{|\widetilde{n}(G) + n''(r')|}{|r-r'|}$$

As of the last term is the short-ranged pair between the atoms

$$U_{R,R'} = \frac{1}{2}\int dr \int dr' \frac{(n'_R(\mathbf{r})n'_{R'}(\mathbf{r}'))}{|r-r'|} \tag{2.116}$$

Both the potential $\overline{v}$ and pair potential $U_{R,R'}$ have non-spherical terms and adjust to the actual charge density [26], [25].

Chapter 3

Ti-Si-C MAX Phase

3.1 Introduction

More attention has been given to both the ternary and binary phases belonging to the Ti–Si–C system. This is due to their thermodynamic stability and various applications ranging from microelectronics (SiC), thin film coatings and the mechanical industry. The TiC thin film coatings are wear-resistant and hard. The Ti-Si-C system is made up diffusion couples of the type $Ti_xSi_{1-y}C$. Research shows other various phases such as $\beta-$Ti,$Ti_5Si_3C_x$ and TiC_{1-y}. Of particular interest in this work is Ti_4SiC_3, Ti_3SiC_2, TiSiC ternary phases of this system with $(Hf/Zr)_3TiC_2$ also included These all represent "MAX" phases with a general formula $M_{n+1}AX_n$ where: *M(early transition metal), A (an element from IIIA and IVA groups)* and *X (either nitrogen or carbon)* in this case carbon. This system has a combination of Ti, Si

which yield hard and brittle solids, but when combined together with carbon, forms a soft binary compound Nowadays TiS powder is being produced commercially.

3.2 Crystal Structure

In this work we are generalizing the crystal structure of MAX phases. The crystal structure of all the max phases is similar with minor disparities. However all posses the same layered hexagonal structure, and are nanolaminars except for Ti_3SiC_2 which has been argued by Ahuja *et al.*, to be isotropic [27]. Each crystal system has 4 basis vectors, 3 which are coplanar (*they are not linearly independent and the angle between any 2 vectors = 120^o*). This type of hexagonal system is a *close - packed* structure *(each atom is surrounded by six other atoms in the same plane)* [10], with three neighbors, above and below the plane bringing the total to 12. For those phases that have the *hexagonal close packing* (*hcp*) - the atoms above and below the central plane occupy identical positions. The phases that have a *face centered cubic* structure or are *hexagonally closed packed* have low index planes with simple 36 tilings. These tilings especially their stacking sequence describes the polytypes of the wide band-gap of the semiconductor. The fcc is also known as the cubic close - packed structure (*ccp*) [9].

Since these materials possesses the characteristics of semiconductors, this means in their hexagonal system, the electron states exist in energy bands separated by gaps with no electronic states. The origin of these gaps is explained by band theory

and hybridization in order to form bonding and anti-bonding orbitals separated by twice the hybridization energy, ϵ_n. When many atoms are brought together to form a crystalline solid, the bonding and anti-bonding states, can determine whether a gap persists or the bands overlap. This helps us to make a distinction between metallic, semiconducting or insulating behavior by measuring the size of the band-gap, ϵ_g *(the band-gap is measured from the top of the lower band to the bottom of the upper band).* The 211 max phases (Ti_2TlC, Zr_2TlC, Ti_2AlC and Hf_2TiC) are layered with a layered hexagonal ,close-packed structure [10]. Crystallographically, the 312 max phases (Ti_3SiC_2, Ti_3GeC_2, Zr_3SiC_2, Hf_3SiC_2, Ti_3AlC_2) are described as layers of A atoms with intercalated layers of binary carbide or nitride octahedra. The A atoms that are in the 2_b positions are carbon atoms in position $4f$ ($\frac{1}{3}$, $\frac{2}{3}$,z_c) All these phases, n =1, 2, 3, crystallize under hexagonal structure with large values of c/a *(i.e. equilibrium lattice constants,a and c).* For titanium (Ti), there are two unequivalent atoms denoted Ti $^{(1)}$ and $Ti^{(2)}$ located at the Wyckoff positions $2a$ and $4f$ = ($\frac{1}{3}$, $\frac{2}{3}$,z_{T12}). But the the coordinates $\mathbf{z}_{\mathrm{Ti_2}}$and $\mathbf{z}_c$ are the only free parameters in the crystal structure [7].

3.2.1 Ti_3SiC_2

Ti_3SiC_2 is a layered-ternary carbide with low density, easy machinability, damage tolerance, high modulus, and high temperature oxidation resistance. Raw materials such as Ti/Si/C, Ti/Si/TiC, Ti/SiC/C, Ti/Si/C/SiC, and Ti/SiC/TiC have been

use to fabricate Ti_3SiC_2 ceramics. Titanium Silicon Carbide (Ti_3SiC_2) has a unit cell consisting of silicon layers between which titanium-carbon-octahedra which causes plasticity. This plastic behavior is weak interaction between layers comprising of Ti_6C octahedra, and plane nets of silicon atoms [1], [10]. The unit cell is about $10\mathring{A}$ in size with a stoichiometry 3:1:2 (three titanium, one silicon and two carbon atoms). There are double layers of TiC octahedra interleaved with single layers of Si, and titanium silicides (Ti_xSi_y) resulting in the softness property of this material [28],[12], [29]. There are two atoms per unit cell all in the Si structure (*i.e. the sixfold ring of the Si- structure*). This compound belongs to a P63/mmc space group with a =3.0675$\mathring{A}$ and c =17.657$\mathring{A}$. It has a high Young's modulus and the bulk modulus is thermally stable in argon atmosphere up to at least 1800^{o}C and a good temperature strength [30]. The Young's Modulus, E_{RT} and shear, μ, moduli measured ultrasonically in the 90-300K temperature range were 322$\pm$ 2 and 133.6$\pm$ 0.8 GPa respectively. Both moduli slowly increase and level out at temperature below $\approx$130K [31]. It can be thermally sprayed using high-velocity *oxy*-fuel on steel and metallic substrates. These coatings have resistance to corrosion [32].

When Barsoum [1] and El-Raghy [33] fabricated Ti_3SiC_2 they proposed that $Ti_5Si_3$and TiC are part of the formation of Ti_3SiC_2 contrary to Klemm *et.al.*,'s [34] report that Ti_5Si_3 and TiC formed when using Ti/Si/C/SiC as impurities in the products. Jeitscho and Nowonty [29] also synthesized Ti_3SiC_2 using a chemical reaction between TiH_2, Si, and graphite at 2000^{o}C. Ti_3SiC_2 is a low cost raw material

with ceramic properties, such as a high melting point, resistance to high-temperature oxidation, and resistance to aggressive environments [35]. It does also posses the plastic-like behavior unusual for non-metallic materials. This material stretches out the properties of ceramic constructional materials. This material is advantageous in the manufacturing of ceramic armor material and chemical and petrochemical industries do use it as a superalloy. Another property is its ductile behavior under stress due to the hexagonal crystal structure and Ti-Si bonds (see Figure (3.2)). The Ti_3SiC_2 materials can be treated as potential plastic ceramics at room temperatures. Other applications of these new materials *(e.g. cutting tools, aerospace engines, or as composite materials in the aircraft industry)* are very promising [36],[37], [38],[39],[40]. Its self-lubricating an advantage for rotating electric contacts for **AC** motors and more promising ceramic engines [41]. Ti_3SiC_2 has a lower bulk modulus than titanium carbon (TiC) [12]. Also TiC in Ti_3SiC_2 shows the mobility of the $A-$ group element layer and its conduction by overlapping $4s, 4p$ and $3d$ bands of Ti. This makes Ti_3SiC_2 the most conductive compared to others. This material is non-susceptible to thermal shock [42],[41]. The high heat formation makes it excellent for self-propagating high - temperature synthesis *(SHS)* [28],[41]. However, the electron mobility in TiC_x is higher than in Ti_3SiC_2 showing the scattering potency of the Si atoms in Ti_3SiC_2 [41].

This compound has stacking faults defects and dislocations. These cause plastic deformation either as microscopic deformation or permanent macroscopic deforma-

tion, resulting in bending, compression and tension of the material. Since Ti_3SiC_2has a brittle nature at room temperature deformation is by kink bands [32]. It has a property of high damage tolerance of Ti_3SiC_2 due to induced cracking of the Vickers indentation. Another discovery about Ti_3SiC_2 is the mechanical property because of basal slips confined to the basal planes at low temperatures [32]. There is parallelism in the arrangement of basal planes to the surface and causes the development of kink bands. The delamination between the basal planes, results in plastic deformation when there is constraint in kink - band formation for this material [32],[9]. The plasticity is fully reversible at negligible thermopower (Θ) (*its zero over an extended temperature range of at most between 300K to 850 K*). An estimated value of $\Theta = 0.18\pm\ 0.22\mu\ \mathrm{VK}^{-1}$ has been stated. This negligible thermoelectric power is because of both electrons and holes which are responsible for the conductivity property of the Ti_3SiC_2. Another view is the vanishing of this thermopower (Θ) because of having oppositely charged particles [43]. The implications of these findings are that mobility, concentration and heat transport values of the holes and electrons are identical over a certain range of temperature [1]. This shows that Ti_3SiC_2 *might* be applied for high temperature thermocells [44]. This material is also isoelectronic [7].

Hybridized bands are from Ti $3d-$, C $2p$- states and $Ti^{(2)}$ $3d-$, A $p-$ states. As for the valence bands they are divided into a low energy group with metalloid d-states of $s-$ symmetry and valence bands of (Si,C)$p-$ and Ti $3d-$ states. The carbon (C) and silicon (Si), $s-$ like bands have been found not to overlap. The energy dispersion, of

the Si bands is larger than for C bands due to $3s-$ and $3p-$ orbitals of silicon. Energy location and width of C $2s$- and C $2p-$bands are close to those of TiC though the energy gap between (C,Si)$s-$ and (C,Si)$p-$ bands of Ti_3SiC_2 is very small [41]. The valence states in TiC and Ti_3SiC_2 differ with the crystal field splitting into two states the bonding t_{2g} and anti-bonding state. There are d-d π like Ti-Ti metallic bands in $Ti^{(1)}$ and $Ti^{(2)}$ planes integrated by hexagonal layers of C and Si atoms. In TiC, the $Ti^{(1,2)}$ C interaction in Ti_3SiC_2 has a strong covalent $p-$, $d-$ nature and a weaker Ti-Si interaction. Also the Si-Si bond form a strong covalent bond inside Si monolayers, contributing to high plasticity of Ti_3SiC_2-based ceramic materials.[41]. There is also a combination of hybridized states of Ti $3d-$ orbitals of the e_g symmetry, below the Fermi level (E_f) and also C and Si $p-$ orbitals. The Fermi Level (E_f) is outside the pseudogap with anti- bonding orbitals below , dominated by Ti $3d-$ orbitals of the e_g symmetry and C and Si $p-$ states [32].

Ti_3SiC_2 is very incompressible and its hardness is comparable to that of quenched high carbon steels [45]. Ti_3SiC_2 is fatigue-resistant compared to extension cracks of any single-phase ceramic not under phase hardening transformation [32]. Ti_3SiC_2 decomposes to Ti_3C_2 and silicon (Si) and can be transformed to a more condensed state [45]. Its damping properties are higher than those of other structural ceramics. Ti_3SiC_2 and ordinary water ice also have very similar mechanical properties. They both deform by similar microscopic mechanisms [45].

3.2.2 $(Zr,Hf)_3SiC_2$

The Zr-Si-C system belongs to the ternary phase which is used for ceramic joint microstructures. Zirconium (Zr) on its own is a reactive metal used for brazing alloys so as to improve wetting of ceramic components during joining. Zr-silicides have been investigated and found to be similar to Ti-silicides such as Zr_3Si and Ti_3Si, ZrSi and TiSi as they have the same structural arrangement of atoms. Experimentally the compound Zr_3SiC_2, with 50 at % Zr, 16.7 at % Si and 33.3 at% C, is used as the initial sample resulting in the formation of Zr_5SiC_2 as a matrix phase. Further results showed that the "fictitious" Zr_3SiC_2 compound is expected to be where there is a ZrSi-ZrC tie or ZrSi-SiC-ZrC_{1-x} and ZrSi-$Zr_5Si_3C_x$-ZrC_{1-x} regions [46]. After thorough experimental investigations Y.Wang *et al*, concluded that there's no phase Zr_3SiC_2 or formation of such a compound [27].

Theroretically Zr_3SiC_2 has been modelled using VASP and k-points mesh of 69 or 413 and has the largest volume compared to Hf_3SiC_2 and Ti_3SiC_2 [47],[27]. Also in this work we have done calculations on Zr_3SiC_2 and Hf_3SiC_3 and the results of them both are shown in the results. It has been investigated experimentally and found that " there is no phase analogous to Ti_3SiC_2 in the Zr- Si -C system" despite the theoretical expectations that Zr_3SiC_2 may be the structure. However, the electronic structure of Hf_3SiC_2 is shown on the electronic structure sections.

3.2.3 Ti_4SiC_3

Ti_4SiC_3 also belongs to the 413 group of MAX phases. So far it has been synthesized as thin films for various applications. Unlike the other max phases that has both metallic and plastic properties, this compound tends to have carbidelike properties and less metalicity [48]. Ti_4SiC_3 is has been found to be the mirror image of Ti_3SiC_2, because of the differences in the titanium carbon layers [10], [49]. These Ti-C-Ti sheets are separated by the Ti-Si-Ti sheets with weaker bonds. Previous experimental and theoretical work shows that it is expected to be harder than Ti_3SiC_2 as it has softer TiC.

This compound has larger fraction of the strong Ti-C bonds and Ti-Si bonds, which contribute to its wear performance and friction properties. Also the Ti-Si chemical bonds for its physical properties are weaker than those of Ti_3SiC_2. The TiC is less tense because of the Ti - C bonds though they are weaker for the Ti_3SiC_2. However both Ti_4SiC_3 and Ti_3SiC_2 have stronger Ti $3d$ C $2p$ bonds compared to the Ti $3d-$ Si spd bonds and have a strong covalent bond [48], [49]. It is the Ti $3d$ states that are responsible for the conducting characteristics of the sili-carbide, especially those closer to the Fermi level (E_f) [49].

These $3d$ sites the are responsible for the Ti $3d$- Si $3p-$ bonding. Experimental results show that these Ti $3d$ states hybridize differently with Si compared to the Ti_3SiC_2. Experimental results using, SXE (soft x-ray emission) spectroscopy show that Ti_4SiC_3 and TiC have similar shapes as both have carbidelike attributes. It has

been found to be more similar to TiC even though its the electronic structure shows that it is a mirror image of Ti_3SiC_2 [27],[49]. As max phases have been found to have two different X sites, X_1 and X_{11}, the Ti_1 -C_{11} bonds are shorter than the Ti-C bonds indicating that the Ti- C- Ti sheets are stronger than the TiC, since the Ti-Si bonds are weaker and transfer charge to the Ti - C bonds [47],[27], [48].

3.3 Results and Discussion

Table (3.1) shows the lattice parameters of the computational calculations done in this work and by Sun *et al.*,[50], Holm *et al.*,[51], Yu *et al.*,[52], Hug *et al.*,[53] and Barsoum *et al.*,[1]. Both the LDA and GGA results are shown in the table (3.1), with the GGA results are in brackets. These lattice parameters are for an optimized phase, with a k-point mesh of 69. As is expected the GGA parameters for both c and a are greater than the LDA.even though at times the results are contrary especially as shown in table (3.1). There is a 1% difference, when comparing these results to the experimental results as is with other calculated results. Some of the results such as Hf_3SiC_2 are not available and Zr_3SiC_2 as both the experimental investigations are yet to be performed by others. The results of $\beta-Ti_3SiC_2$ show that , it is more stable than both our work and the $\alpha-Ti_3SiC_2$ as is shown by the lattice parameters.

Table (3.2) shows work done and results obtained for the elastic constants. All these results are work done by Sun *et al.*,[50], Yu *et al.*,[52] and Holm *et al.*,[51]. Table (3.2) serve as guideline for work that might be done on these compounds

Table 3.1: Phase, lattice parameters a and c

Phase	Lattice	
	c(Å)	a(Å)
TiC	7.994(9.71)	3.30(3.06)
SiC	6.141(12.886)	3.081(2.343)
Zr_3SiC_2(This work)	18.679(18.926)	3.301(3.349)
Hf_3SiC_2(This work)	17.688(18.659)	3.116(3.297)
Ti_4SiC_3(This work)	22.310(22.676)	3.02(3.07)
Ti_4SiC_3(calc.)	22.675(22.622)	3.05 (3.08) [48]
Ti_3SiC_2 (This work)	17.726(17.445)	3.0235(3.0746)
$\alpha-Ti_3SiC_2$(*calc.*)	17.701	3.078 [50]
$\beta-Ti_3SiC_2$(calc.)	18.108	3.073 [50]
$\alpha-Ti_3SiC_2$(*calc.*)	17.72	0.308 [51]
$\beta-Ti_3SiC_2$(calc.)	18.07	0.306 [51]
Ti_3SiC_2(exp t.)	17.657	3.0675 [1]
Ti_3SiC_2(exp t)	17.66	3.06 [51]

Table 3.2: Calculated elastic constants Cij(GPa)

Phase	c_{11}	c_{12}	c_{13}	c_{14}	c_{33}	c_{44}
$\alpha-Ti_3SiC_2$(*calc.*)	372	93	110		395	173[50]
$\beta-Ti_3SiC_2$(calc.)	419	55	92		413	165[50]
$\alpha-Ti_3SiC_2$(*calc.*)	360	84	101		350	158[52]
$\beta-Ti_3SiC_2$(calc.)	360	86	89		348	120[52]
Ti_4SiC_3(calc.)	365	125	120	-10	375	122[51]

Table 3.3: The bulk modulus B, pressure B', total energy E, and total volume

Phase	B_v(GPa)	B'(GPa)	E_0(eV/atom)	V_0(Å^3)	Toatal Volume(cm^{-3}
TiC	124(80)	3.924(1.177)	-15.37(-15.55)	267.58(318.52)	79.27(94.39)
TiC(calc)	350 - 400[1]				
SiC	111(264)	3.785(3.931)	-15.37(-8.41)	266.96(262.05)	79.09(77.63)
Hf_3SiC_2	181(205)	4.295(4.021)	-9.82(-10.67)	98.85(94.09)	175.72(167.25)
Zr_3SiC_2	184(166)	4.293(4.330)	-9.84(-9.04)	99.15(103.50)	176.25(183.98)
$Ti3SiC_2$	207(183)	4.02(4.38)	-9.57(-8.75)	77.69(84.61)	138.11(145.13)
Ti_4SiC^3	220(207)	4.34(4.38)	-7.94(-8.90)	97.90(73.90)	177.13(175.17)

Table (3.3) is the bulk modulus (B_v), pressure (B'), total energy (E) and total volume obtained from the calculations from this work. These results are within the same range of both the experimental and calculated results of LDA and GGA. GGA results are in brackets. Ti_4SiC_3 has the highest total volume and is expected to be harder than the others especially Ti_3SiC_2. The bulk modulus for Ti_3SiC_2 compared to both $(Zr/Hf)_3SiC_2$ is higher, but has been expected to be in the same range as $(Zr/Hf)_3SiC_2$ since theoretical calculations predict these three compounds to be from the same family although experimental findings are proving otherwise so far [52],[51].

Table (3.4) shows work from Sun *et al.*,[50], Holm *et al.,* [51], Yu *et al.*,[52], both experimental and calculated results.

The two polymorphys α and β of Ti_3SiC_2 were used for comparison in this work because of their hexagonal symmetry like Ti_3SiC_2 with space group of $P6_3/mmc$. Analysis based on Bader's quantum theory of "atoms in molecules"(AIM), a theory about bonds, structures atoms and crystal stability showed that the Ti- Si bonding effect of the beta is weaker than the alpha, making the beta less stable even though Si

Table 3.4: The bulk modulus(B), shear pressure(G) and elastic modulus(E) for both alpha and beta Ti3SiC2 and Poisson ratio

Phase	B_v(GPa)	G_v(GPa)	E(Ry)	υ
$\alpha-Ti_3SiC_2$(calc.)	196	152	362[50]	
$\beta-Ti_3SiC_2$(calc.)	192	170	394[50]	
Ti_3SiC_2(calc.)	204	123	368	0.25[51]
Ti_3SiC_2(expt.)	179-185	133-142	322-339	0.20[51]
$\alpha-Ti_3SiC_2$(expt.)	185	139	333	0.20[52]
$\alpha-Ti_3SiC_2$(expt.)	187	142	339	0.20[52]
$\alpha-Ti_3SiC_2$(expt.)	179	134	322	0.20[52]
$\alpha-Ti_3SiC_2$(expt.)	181	136	337	0.20[52]
$\alpha-Ti_3SiC_2$(expt.)	206	131	329	0.20[52]
$\alpha-Ti_3SiC_2$(calc.)	182	142	338	0.191[52]
$\alpha-Ti_3SiC_2$(calc.)	177	129	311	0.207[52]

- C bonds do provide additional stabilization for the beta. Ti_3SiC_2, the bond lengths show that of the Ti1-C bond is longer with a smaller electron density compared to Ti2-C bond for both α and β.This is due to weaker Ti2-Si bonding relative Ti2-C bonding. The aim of the comparison of our Ti_3SiC_2 with both α and β was to estabilish whether the Ti_3SiC_2 we were using is $\alpha-Ti_3SiC_2$ or $\beta-$ Ti_3SiC_2.comparing both the LDA and GGA results of its bulk, shear moduli and the total energy with those of the polymorphs even though the two polymorphs have been found to differ in structure [52].

3.3.1 Electronic Structures

In this section we initially look at the comparison of Ti_4SiC_3 and Ti_3SiC_2 max phases electronic structures, though they don't belong to the same group. Part of this research was carrying out the ab – initio calculations of both Ti_4SiC_3 and Ti_3SiC_2 in

order to determine their electronic structures. Experimental work by Magnuson *et al* [54] on the electronic structure and chemical bonding of this 413 phase has shown that it is a mirror image of the 312 phase Ti_3SiC_2. As it has been pointed out before, figure (3.1), shows the relationship between the weak and strong bonds of Ti-Si and Ti-C respectively and how they are situated in the Ti- Si- C system in relation to their interaction with the Ti- Si - Ti sheets. Also clearly seen is the how the softer Ti- Si - Ti sheets with weaker bonds separate the Ti- C- Ti bonds in Ti_4SiC_3.As a result of this arrangement Ti_4SiC_3 had been found to be harder than Ti_3SiC_2.

As the Si monolayers in the Ti-C matrix replace the Ti- atoms they lose some bond strength to the nearest - neighbor Si atoms which to some degree compensate with the Ti- C bond. However more results show that the Ti- Si peak of Ti_4Sic_3 is less intense closer to the Fermi level than in Ti_3sic_2. In Ti_4SiC_3, the Fermi level is close to the region with a low density states (pseudogap) as experimental results show [50] .

The 413 has been found to have a lower conductivity than the 312 system due to the decrease in metallicity in the pseudogap [35]. The elastic modulus (E) increases with decreasing number of Si layers per Ti layer. The hardening of the 413 phase is due to the changes in the bonding conditions of the weaker Ti – Si bonds. This surprisingly makes Ti_4SiC_3 more similar to TiC than Ti_3SiC_2, since there is a reduced number of inserted Si monolayers [35].

It should be noted that the number of Si- layers per Ti layers in the Ti – Si – C

system does affect both the physical properties and the electronic structure [47].

Unlike in Ti_3SiC_2, the C atoms are replaced by Si layers and the Ti-Si-Ti sheets separate the Ti-C-Ti sheets. Figure (3.2), and figure (3.3) show both Ti_4SiC_3 and Ti_3SiC_2 crystal structures separately.

Figures (3.2),(3.3) show that Ti_4SiC_3 is the mirror image of Ti_3SiC_2, with the Ti -C -Ti slabs, replaced by Ti-Si-Ti slabs.

Figure (3.4) and Figure (3.5) have similar structural arrangement of the (Zr,Hf) - C and Si - C atoms even though Zr_3SiC_2 is upside - down. The silicon layers are between (hafnium,zirconium)-carbon-octahedra. Both $(Zr, Hf)_3SiC_2$ show many similarities to the structural arrangement of atoms in Ti_3SiC_2. $(Zr, Hf)_3SiC_2$ can be used as a substitutes for Ti_3SiC_2 since zirconium has similar applications with titanium as all of them are transition metals. More similar properties might be in their bond strengths, elastic properties, ductility, resistance to corrosion, conductivity of both heat and electricity and plasticity. Here the double layers of TiC octahedra are interleaved with single layers of (Zr, Hf) in place of Si atoms,and titanium silicides (Zr,Hf_xSi_y) resulting in the softness property of this material. Other properties such as susceptibility to kink bands and defects might be a little bit different considering where there elements are situated in the periodic table.

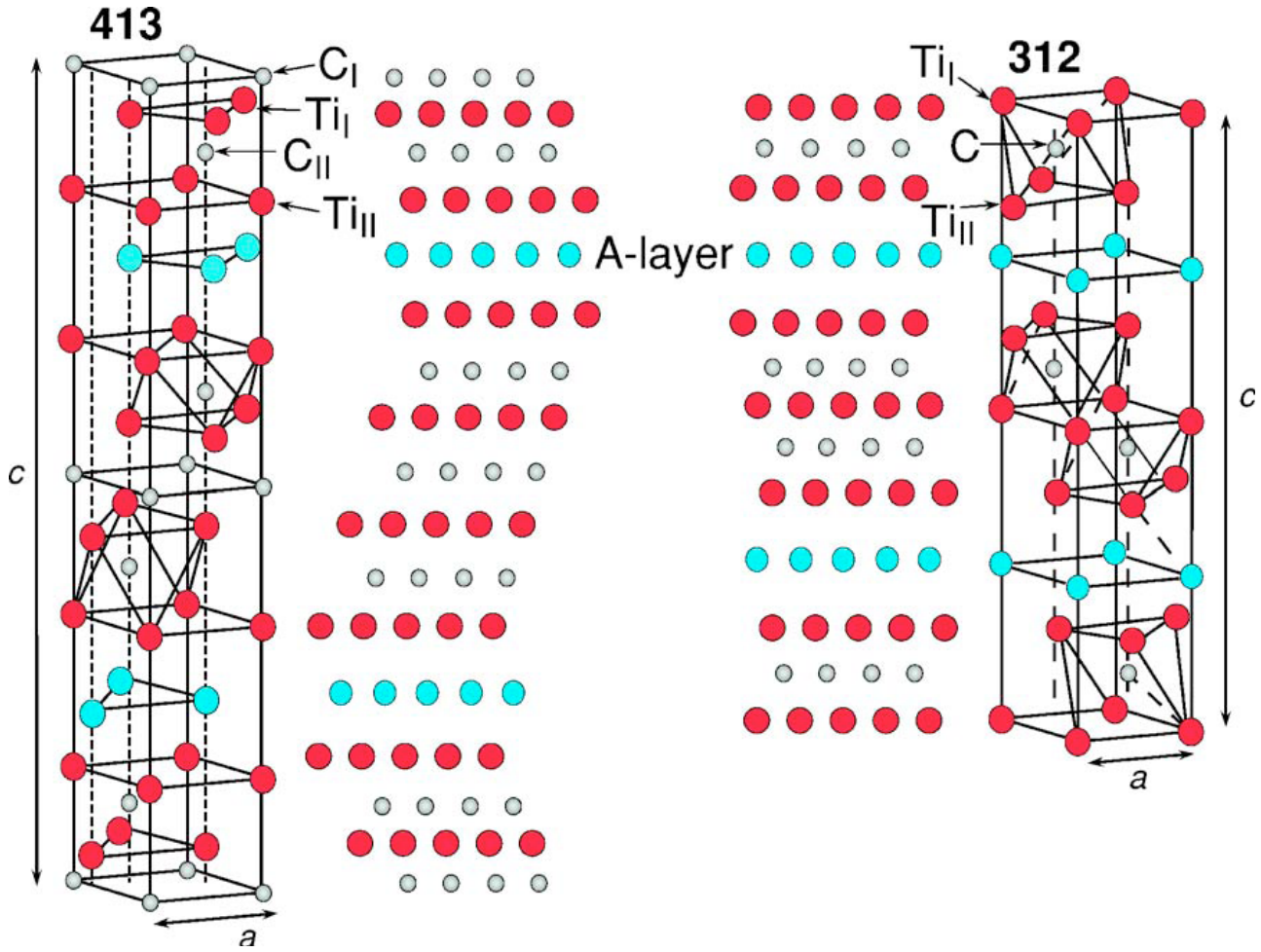

Figure 3.1: The hexagonal crystal structure of 413 Ti_4SiC_3 compared to crystal structure of 321 Ti_3SiC_2 [2].

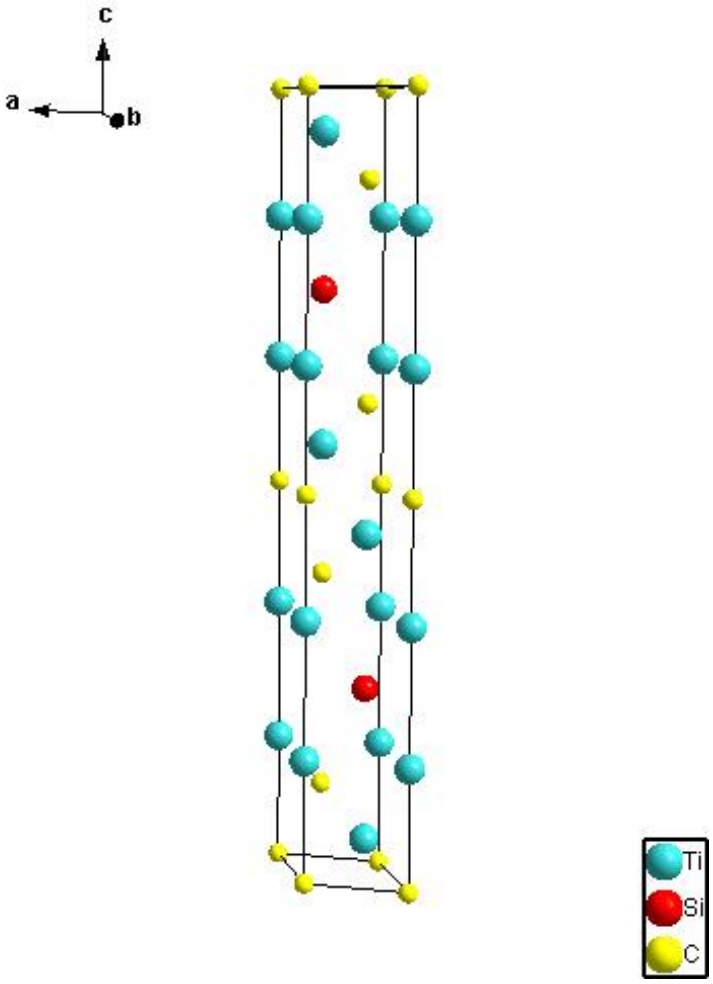

Figure 3.2: Hexagonal structure of Ti_4SiC_3(413)

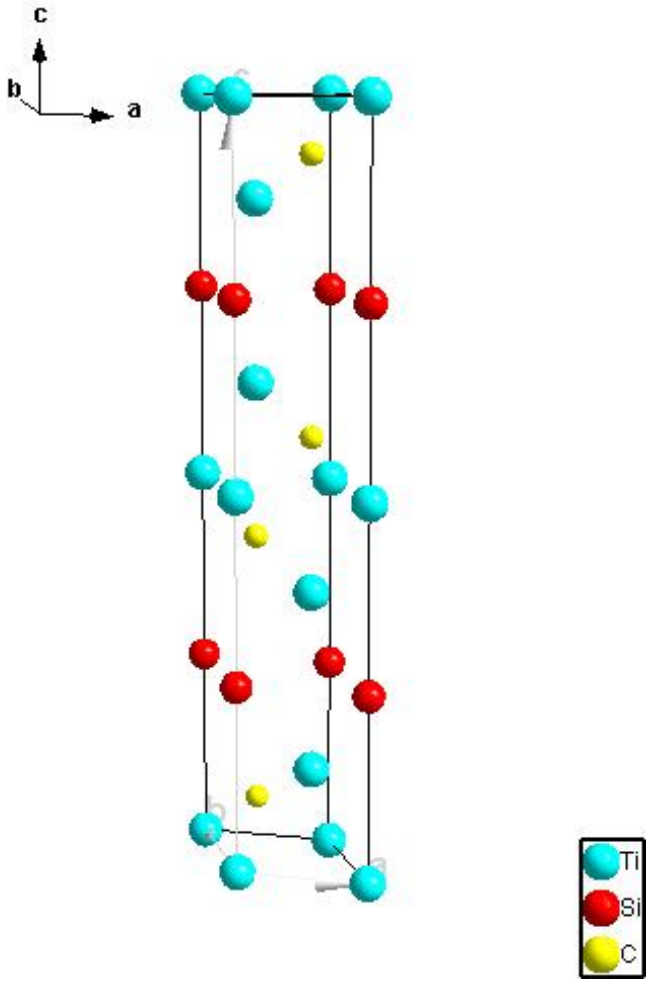

Figure 3.3: Hexagonal structure of Ti_3SiC_2(321)

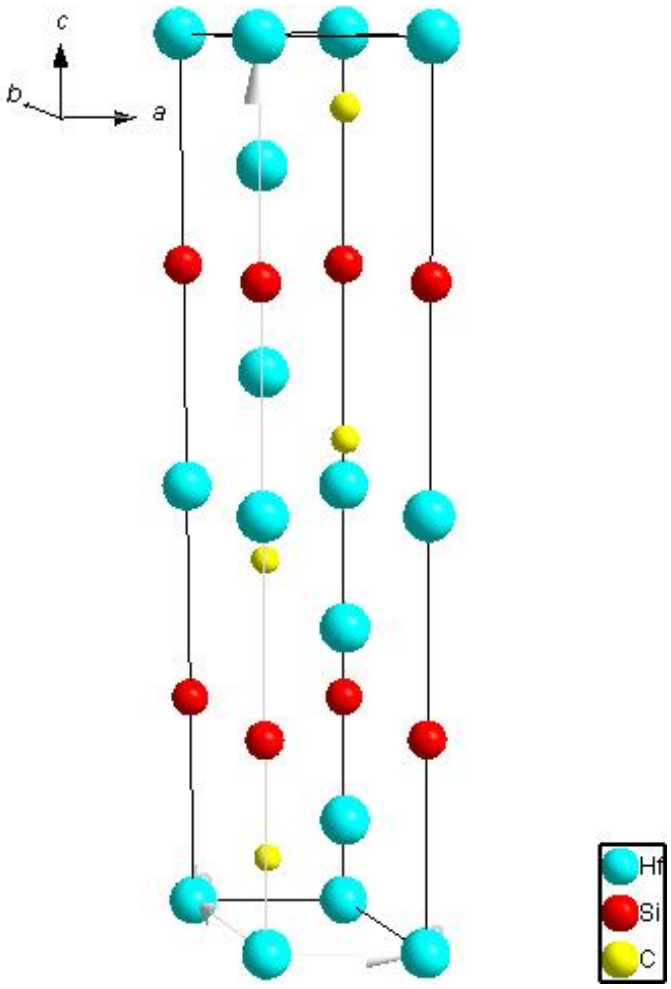

Figure 3.4: Hexagonal structure of Hf_3SiC_2(321)

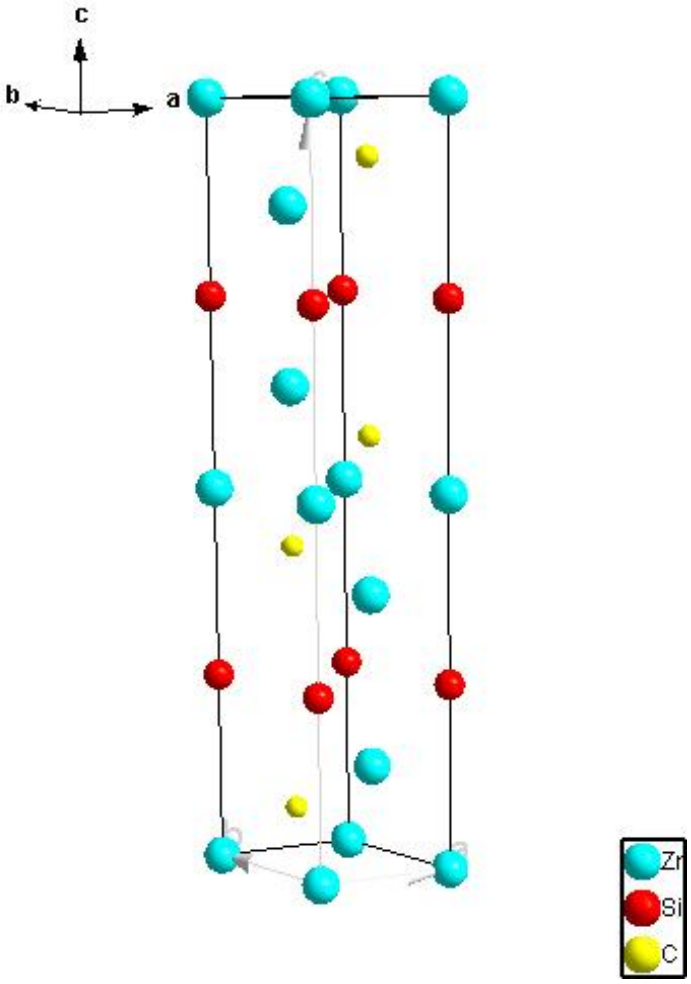

Figure 3.5: Hexagonal structures of Zr_3SiC_2(321)

3.3.2 Density of States Plots

There is a pattern of visible peaks on the -40 to -20 energy range (x-axis) on all these graphs. This shows the available states for occupation at that energy level. This pattern continues from the -10 to 10 region with lower peaks, except for Zr_3SiC_2. For $(Ti)_{3/4}SiC_2$, this confirms the experimental findings of a high peak TiC at the low energy levels as most of the bonding properties are from titanium carbon (TiC) which has C *s*-states. It further posses valence and conduction bands that are said to feature hybridized C $p-$ orbitals and Ti d- orbitals. Barsoum *et.al.*, found the density of states (DOS) near the Fermi level E_F to be 0.83 eV Ti atom^{-1} and is comparable to stoichiometric TiC.

Comparing results done in this work and those from others, they do correlate [2]. See figure(3.7)

More experimental results done by others using, SXE spectroscopy show that Ti_4SiC_3 and TiC have similar shapes as both have carbidelike attributes. Ti_4SiC_3 has been found to be more similar to TiC even though it has an electronic structure shows that is a mirror image of Ti_3SiC_2.

For $(Zr,Hf)_3SiC_2$ the is no difference between the two. This could mean then it is not only Zr_3SiC_2 that is the mirror image of Ti_3SiC_2, Hf_3SiC_2 could also be.

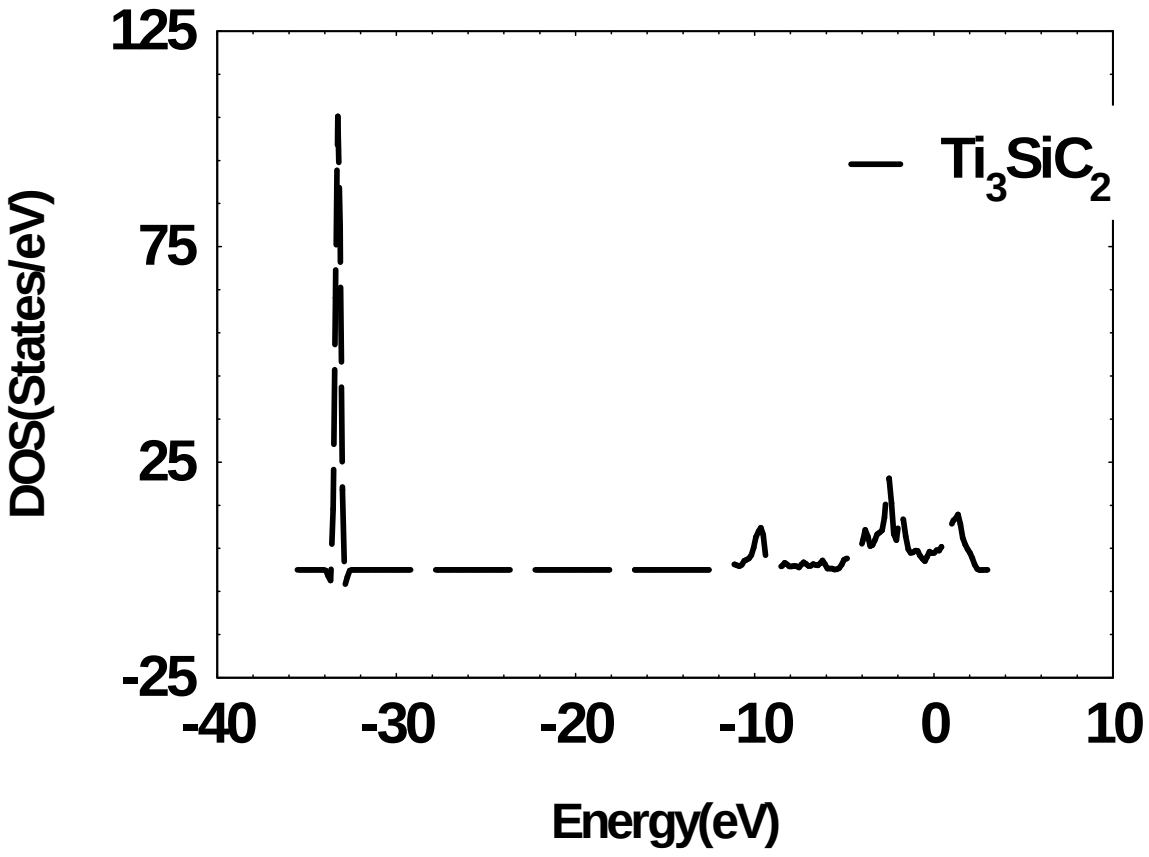

Figure 3.6: Calculated DOS for Ti_3SiC_2. Fermi level is at zero

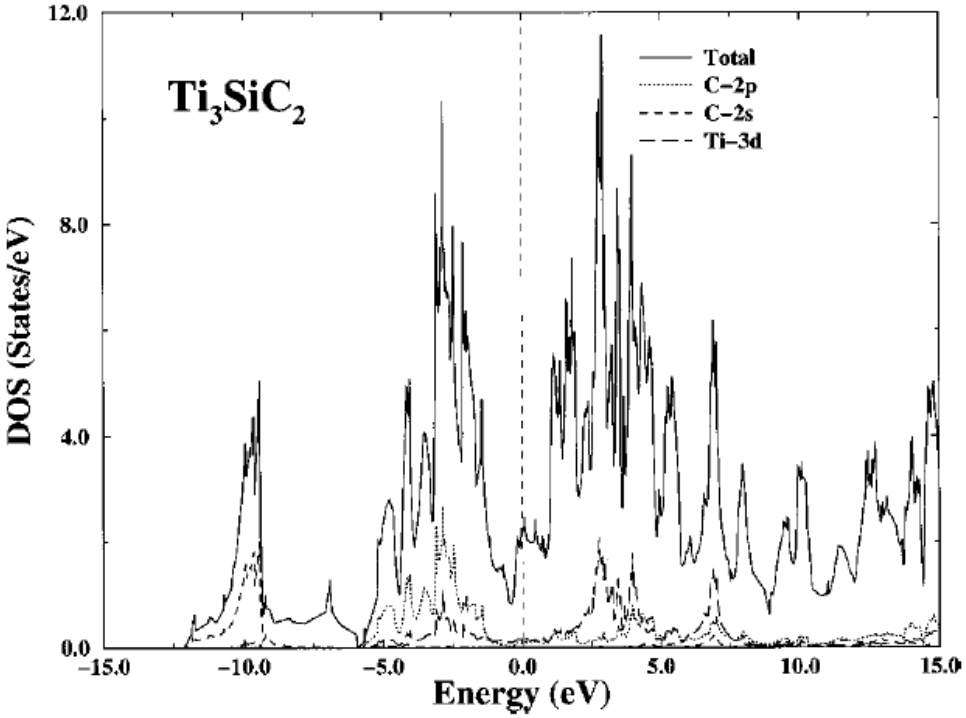

Figure 3.7: Calculated density of states for Ti_3SiC_2 full line shows total DOS, while the long - dashed dotted and dashed lines show the Ti $3d$ - partial, C $2p$-partial and C $2s$-partial DOS respectively. The Fermi level is set at zero energy and marked by a vertical dotted line [2]

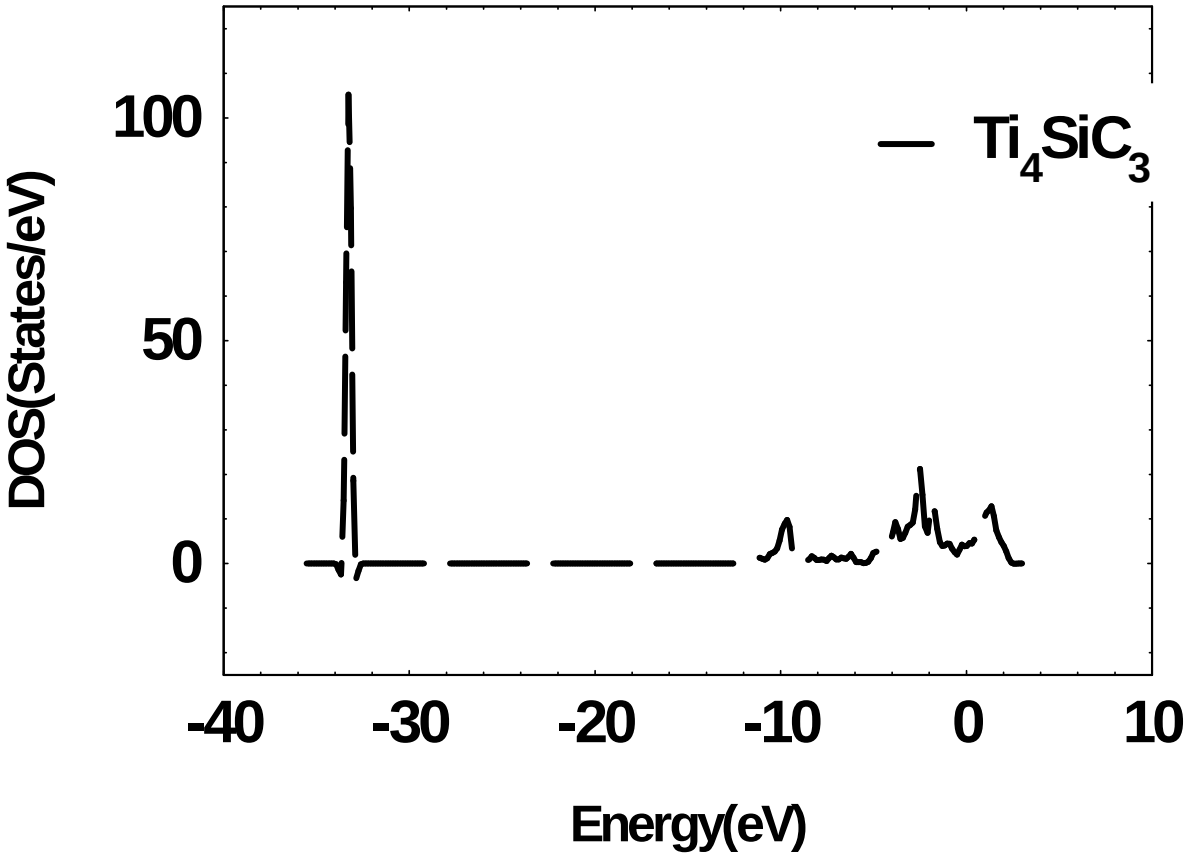

Figure 3.8: Calculated DOS for Ti_4SiC_3. Fermi level is at zero

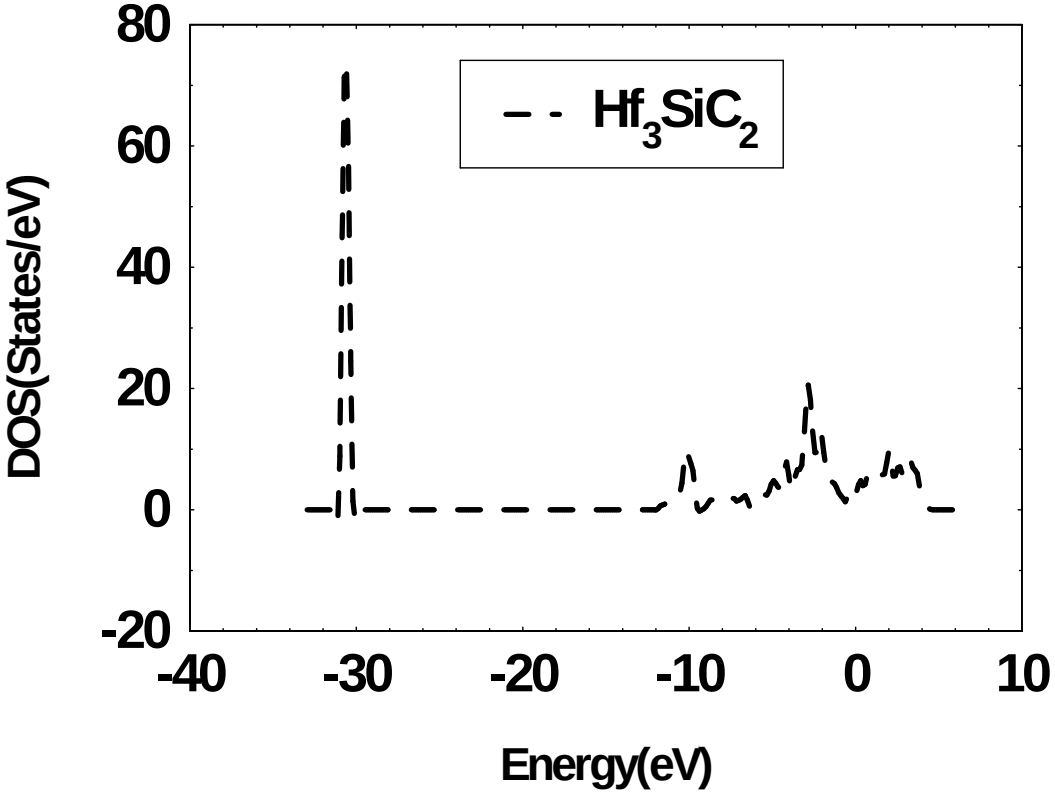

Figure 3.9: Calculated DOS for Hf_3SiC_2. Fermi Level is at zero energy

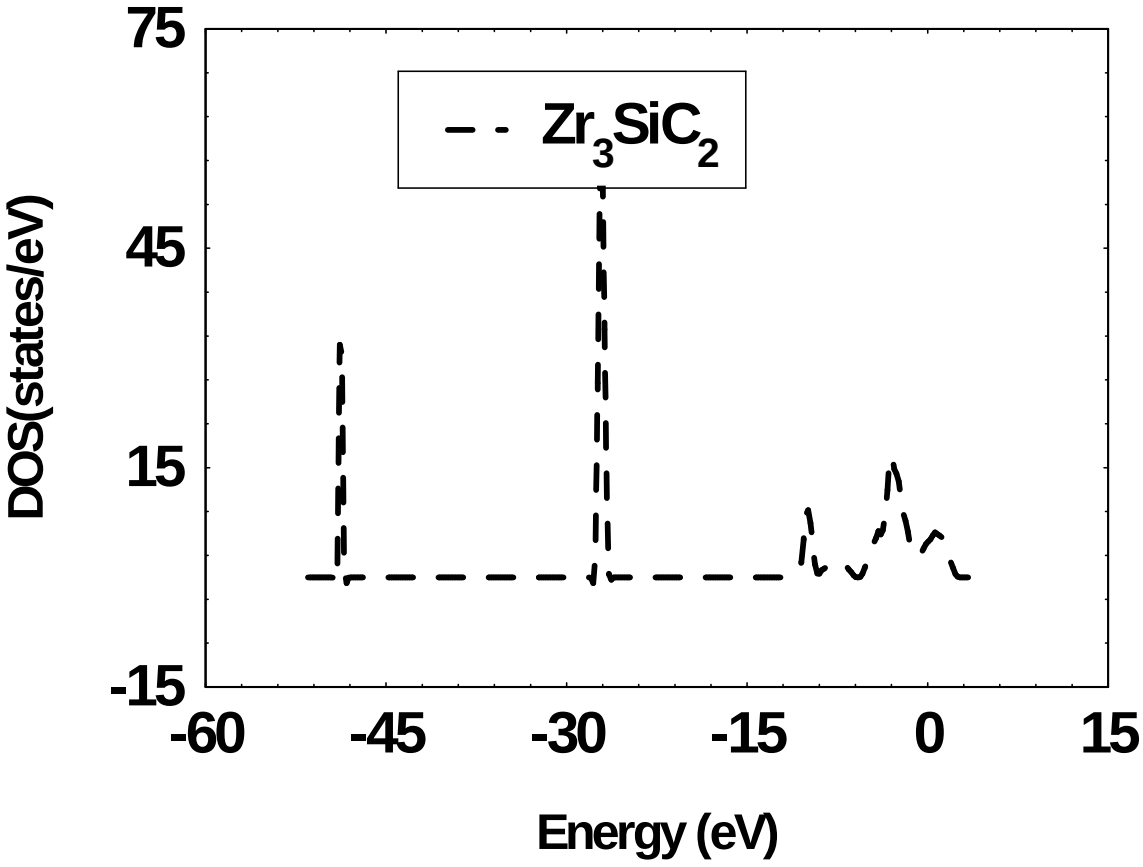

Figure 3.10: Calculated DOS for Zr_3SiC_2. Fermi Level is at zero energy level

Chapter 4

Ti-Al-N MAX Phase

4.1 Introduction

The titanium aluminium nitride (Ti-AI-N) system is part of the most recently sort out material group that has been the center of attention in recent years, the "MAX" phases [55]. This is due to research and development of a variety of important materials especially technological-used materials such as (Ti,AI)N for wear-resistant coatings, TiN for diffusion barrier and Al for metallization for silicon semiconductor devices, high-temperature γTiAl + Ti_2A1N composites, and also $TiAl_3$ + TiN + AlN enhanced Al base alloys [56]. Included on this system is the 211 phase or n = 1 *(* e.g. Ti_2AlN*)* and 413 phase or n = 3 (e.g. Ti_4AlN_3). So far more has been investigated on the three ternary compounds, that are known to exist in this system. These are Ti_2AlN, Ti_3AlN and $Ti_4AlN_{3-\delta}$. The first compound, Ti_2AlN, was identified in

1963 by Jeitschko *et al.*,[29]. Schuster and Bauer [57], later reported two other compounds, Ti_3AlN and $Ti_3Al_2N_2$ [58]. Titanium aluminium nitrides, ($Ti_{1-x}Al_xN$), can be prepared as films by various sputtering methods and form metastable phases [59]. Experimental investigations on thin films show that $Ti_{1-x}Al_xN$ crystallizes in the cubic *(c)* NaCl modification (*space group* $Fm\bar{3}m$) for AlN mole fractions of x $\leq$ 0.7. But when the Al, content is high a mixed *NaCl+ZnS-wurtzite* structure is formed, or the films crystallize completely in the $ZnS - wurtzite$ (w) structure *(space group P63mc)*. However cubic $Ti_{1-x}Al_xN$ is preferred for industrial applications due to the improved mechanical and thermal properties compared to c-TiN and mixed or wurtzite structured $Ti_{1-x}Al_xN$ [60].

Interestingly at elevated temperatures which causes an increase in diffusibility $fcc-Ti_{1-x}Al_xN$ decomposes into stable $fcc-$TiN and $hcp-$AlN especially by nucleation and growth, and this decreases the hardness properties of the system. Also the crystal structure of the ternary Ti-Al-N system along with the wide-ranging solubility of AlN in TiN is typical for the iso-structural group of cubic titanium-based nitrides. Therefore commercially, the $Ti_{1-x}Al_{\ x}N$ coatings succeeded since they not only have superior oxidation resistance, the coatings can self-adapt, to thermal load when cutting is done by age hardening [60]. AlN and TiN are major contributors in the formation of almost all the phases in this system. The Al–N bonds in AlN can be described as predominantly covalent-ionic in nature and the Ti–N bonds in TiN are metallic, ionic, and covalent in nature. Calculated compositions agree with the fact

that the bonding character of this nitride system is a mixture of metallic, ionic, and covalent bonding. For the high-symmetry compounds, where Ti and Al atoms periodically populated the metal sublattice the Al–N bonds are also metallic, ionic, and covalent in nature, while for the TiN bonds the covalent contribution to the overall bond is suppressed [60]. As nitrides, there is a higher electronegativity of N and as well as the strong Ti $3d$- N $2p-$bond which result in stronger ionic contribution, and also the weaker Ti $3d$- Al $3p-$ bond and the Ti $3d$- N $2s$- bonds [48]. Hybridization for both Ti $3d$- N $2p-$ and Ti $3d-$ N $2s$ at the Fermi level is much deeper in energy compared to the hybridization of Ti $3d$- Al $3p-$ and this indicates stronger bonding. If the relatively weak Ti $3d$-, Al $3p$- bonding is strengthened, there will be an increase in the stiffness of the material [59].

4.1.1 Ti_2AlN

Ti_2AlN is one of the two interesting materials from this family and also belongs to a group of ternary nitrides which are of the 211 phase of "max" phases [53],[48]. In the early 1930s the 211-crystal structure was derived when these materials were referred to as Hägg phases ($H-phase$) depending on the ratio of the radii of the constituent atoms [61],[48]. Ti_2AIN is not only an $H-phase$ (Hägg *phase*) material but its also isotopic with Cr_2AlC structure and is the most stable ternary compound in this system. It has been observed to exist over the temperature range from $700\,^oC$ to 1600 ^{o}C, and the melting point is above at least 1950^oC probably above 2500^oC. At

1300^{o}C this compound is homogeneous at the composition of $Ti_2AlN_{0.82}$ [12],[56],[62] exhibiting metallic electrical conductivity with an anisotropic character. The chemical bonding in Ti_2AlN is metallic-covalent-ionic in nature. Polycrystalline Ti_2AlN ceramics fabricated by Barsoum, Brodkin, and El-Raghy using a hot pressing method demonstrated that Ti_2AlN has an excellent machinability property, hardness of 3–6 GPa, electrical conductivity in the range of 2 – 5 x$10^6\Omega^{-1}m^{-1}$, high yield strength, and significant plasticity at high temperatures. These properties are due to the structural properties. Besides these properties, like max phases it is relatively soft (Vickers hardness of 3.5GPa). and it deforms under compression at room temperature which is not detrimental [56],[63].

At higher temperatures or for longer periods, this compound precipitates with a hexagonal crystal structure and has hexagonal lattice constants of $a = 52.99\mathring{A}$, and $c = 51.361\mathring{A}$. The plate- like precipitates are formed at the dislocations of the *H- phase* lying parallel to the $< 111 >$ planes of the TiAl matrix. Schuster *et al.*, state that Ti_2AlN *(H-phase)* is in equilibrium with TiN, Ti_3Al and TiAl at 1237K according to the report of the experimental techniques used by Louiseau *et al.* and examined by Kaufman *et al.* [64],[63]. The space group is $P6_3/mmc$ and the Wyckoff positions are $4f$ for Ti, $2d$ for Al, and $2a$ for N. Researchers Zhou and Sun, showed a $4f$ and $2a$ positions for Ti and the metalloid (N), respectively and $2c$ position for Al instead of $2a$. Similarly the $2d$ $[(\frac{1}{3}, \frac{2}{3}, \frac{3}{4}), (\frac{2}{3}, \frac{1}{3}, \frac{1}{4})]$ and $2c$ positions $[(\frac{1}{3}, \frac{2}{3}, \frac{1}{4}), (\frac{2}{3}, \frac{1}{3}, \frac{3}{4})]$ are actually quite different. In fact each of the $2d$ and $2c$ positions corresponds to a

different stacking of the metals along the c direction. The stacking of the metals in the correct *H- phase* is the classical $ABAB$ sequence of an *hcp* metal with two planes periodicity along the hexagonal axis [53]. The chemical sequence is formed by two titanium planes and one aluminium plane leading to crystallographic sequence of six planes in the unit cell, which can be written as,

$$AB'ABA'B \tag{4.1}$$

where the primes denote the aluminium planes. The metalloid atoms in the *H phase* are located in the octahedral cavities between the Ti planes. The Ti-Al-Ti stacking can be a close packing of a fcc or *hcp* metal. The choice of the $2c$ Wyckoff position for the aluminium atoms leads to the sequence

$$\gamma AB'A\gamma BA'B \tag{4.2}$$

which includes AA stacking sequence. The total energy from this crystal structure is expected to be high or prohibitive. The states of the Fermi level are mainly Ti $d-$ and Al $p-$. The Ti $d-$ electrons are mainly contributing to the density of states (DOS) at the Fermi level and therefore play a role in the conduction properties, although $d-$ electrons are generally considered as low efficient conductors. This is contrary to the Al electrons which do not contribute significantly at Fermi level due to a scooping effect resulting from the presence of the titanium $d-$ states [53]. Projected

densities of states show that bonding in this compound is due to Ti $d-$ N $p-$ and Ti $d-$ Al $p-$ hybridization and the intensity of the total density of state at Fermi level is higher for Ti_2AlN and also has higher electrical conductivity [53]. Researchers have observed that Ti_2AlN has some nitrogen deficiency, with a suggested formula of $Ti_2AlN_{0.8}$. But others have reported the composition is forming in the scales during nitriding as $Ti_{2.04}Al_{0.96}N_{1.09}$ [65].

Ti_2AlN is in equilibrium with all the binary and ternary phases in the Ti-Al-N system except AlN. Like other materials, deformations are present and these deformations are limited because of a lack of sufficient easy slip systems *(rather than the five independent slip systems needed for arbitrary deformation)* and are quite anisotropic. A nitrogen (N) atom provides one more valence electron to the Ti_6N octahedron in Ti_2AlN. Enhancement of the valence electron density causes strengthening of the Ti–Al bonding, which results in the increase of the strength of the material. Electronic structure analysis showed that the Ti–Al bonding states shift below the Fermi level (E_F) to lower energy levels, ranging from -3.01 to -0.55 eV. This indicates a strengthening of the Ti–Al bonds, and thereafter enhances the ideal strengths of Ti_2AlN [66]. Moreover, every second single monolayer of N atoms in TiN is replaced by an Al layer, resulting in under-stoichiometric TiN. The Ti_2N slabs surrounding the Al monolayers are twinned with the Al layers as mirror planes. The crystal structure of Ti_2AlN has thermodynamically stable nanolaminates of binary Ti-N-Ti layers separated by softer Ti-Al-Ti layers with weaker bonds [48].

The Young's modulus *(E)* of a single-crystal thin film of 270 GPa Ti_2AlN is significantly lower compared to TiN with a Young's modulus of 449 GPa. Comparisons of the crystal structures of Ti_2AlN with TiN, clearly shows that the physical properties and the underlying electronic structure of the Ti-Al-N system is strongly affected by the intercalated Al layers. This confirms that TiN and Ti_2AlN generally have more dominating Ti $3d-$, $p-$ density of states (DOS) at the Fermi level (E_F). This contributes to more metallic-like properties of these materials. This intercalation of Al monolayers into the TiN matrix results in the transformation of the character of the Ti $p-$ DOS close to the E_F. Therefore conductivity increases because Al metal is a good conductor. However, the total conductivity is largely governed by the Ti metal bonding and is roughly proportional to the number of states at the Fermi level of TiN, at 0.43eV atom; Ti_2AlN at 0.41eV atom. Thorough experimental results show that AlN can coexist with TiN_{1-x}, Ti_2AlN, and $TiAl_3N$ whereas the ternary nitride Ti_2AlN can be in equilibrium with $TiAl_3$, $TiAl_2$, TiAl, TiN_{1-x}, and Ti_3AlN and the solid solution based on alpha (Ti) coexists with Ti_3Al, Ti_3AlN, TiN_{1-x}, and Ti_2N. The more stable hexagonal phase had a measured stoichiometry of $Ti_2AlN_{0.82}$. If the excess Al is converted to AlN according to the reaction [48],[67].

$$2TiAl_{3(s)} + N_{2(g)} \rightarrow Ti_2Al_{(s)} + 5AlN_{(s)} \tag{4.3}$$

free energy change for the overall reaction is negative, especially at 21429 kJ/mol of Ti_2AlN. These free energy arguments explain the absence of liquid Al and the pres-

ence of a heterogeneous mixture of various nitride phases when the $TiAl_3$ compound is present. Nitrogen must diffuse through the TiN and Ti_2AlN phases and is consumed by reacting at the Ti_2AlN or $TiAl_3$ interface with $TiAl_3$ to form more Ti_2AlN according to the reaction [68].

$$2TiAl_3+0.5N_2= Ti_2AlN+5Al \tag{4.4}$$

4.1.2 Ti_3AlN

This is the 2^{nd} member of the Ti-Al -N system and does not follow the $M_{n+1}AX_n$ formula. The composition ratio of Ti to Al in the perovskite nitride is 3:1 and the nitrogen atoms sit at the octahedral with the needle direction lying along <001> TiAl. Ti_3AlN has a perovskite-type structure and a composition of $Ti_3A1N_{0.56}$ at 1300 ^{o}C and it melts incongruently into either liquid $+\delta TiN_{l-x}$ + Ti_2AIN or liquid $+\delta TiN_{1-x}$ at 1590 $\pm$ 10 ^{o}C. Perovskite Ti_3AlN was also reported to form at the metal-ceramic interface upon joining AlN and Ti at 1200 ^{o}C. However at 1175 ^{o}C or less, it fills a B-type crystal structure and its assumed to have a composition of Ti_3AlN. The formation of this phase is so slowly that it is not recognized at 1000^oC according to experimental research carried out by Schuster and Bauer. In the formation of thin films, annealing at 400 ^{o}C leads to AlN decomposition and diffusion of released Al and N into the Ti layers, with formation of Ti_3AlN. At a low-temperature, below 1200 $^\circ C$ of Ti_3AlN_{1-x}, the cubic perovskite structure transforms to a filled $R_{e3}B-$

type orthorhombic structure, with $a = 0.3065$nm, $b = 1.0748$nm,and $c = 0.8455$nm [56],[65].

4.1.3 $Ti_3Al_2N_2$

In 1984, Schuster and Bauer reported an additional ternary compound in Ti -Al -N system called $Ti_3Al_2N_2$ and claimed it was homogeneous [56],[69]. Its chemical formula composition decomposes above 1335 K, and is unstable at 1200 K or below. No liquid was observed to appear upon heating this compound up to 1900K [56]. The crystallographic and diffraction data, proposes the crystallographic structure of $Ti_3Al_2N_2$ to be a hexagonal unit cell of the space group $P6_3mc$, with lattice parameters of $a = 50.299$nm and $c = 52.33854$nm which was later revised to $P6_3mc$, with $a = 50.2987$nm and $c = 52.3350$nm [55].

Researchers, Lee and Petuskey [70] re-examined the work of Schuster and Bauer [57] over the 900K to 1873K temperature range and, based on chemical analysis and an erroneous interpretation of the X-ray diffraction *(XRD)* results, concluded that $Ti_3Al_2N_2$ was $Ti_3Al_{1-x}N_2$ and it is iso-structural with Ti_3SiC_2. Barsoum and Schuster, however, noted that a c-lattice parameter of 2.3350nm is incompatible with the Ti_3SiC_2 structure. More recent research was done on this compound by Barsoum and co-workers on a simple model where all the atoms are assumed to be Ti, using the high-resolution transmission electron microscopy *(TEM)* chemical analysis and Rietveld analysis of neutron diffraction. Their results showed that the correct structure

stoichiometry was neither $Ti_3Al_2N_2$ nor $Ti_3Al_{1-x}N_2$, but a new phase, Ti_4AlN_{3-x}. This new model had a unit cell composed of ten layers—three layers of Ti atoms separated by two layers of Al atoms, with N atoms residing in the octahedral sites between the layers of Ti atoms [55]. Their results also showed that this compound had relation to the family of layered machinable hexagonal ternary carbides with the general formula $Mn_{1-x}AX_n$, where M is an early transition metal, a group $A-$ element *(mostly III-A and IV-A)*, and X which is either carbon (C) or nitrogen (N). Concomitant electron microprobe analysis *(EMPA)* samples of $Ti_4AlN_{3-\delta}$ determined the chemical composition to be 50.8 at.% Ti, 12.4 at.% Al, and 36.8 at.% N, or 4 :1 : 3, which is almost identical to the one claimed by Lee and Petuskey [69].

4.1.4 Ti_4AlN_3

This ternary nitride Ti_4AlN_3 represents a member of a third family of layered ternary nitrides and Ti-Al-N system. This material is a potential candidate for high-temperature structural applications. At 1000^{o}C it deforms plastically, with a "*yield*" point of 450 MPa. It is relatively soft *(*Vickers hardness 2.5GPa*)* whilst elastically rigid, lightweight (4.6g/cm^3) and machinable. The Young, shear and bulk moduli are 310, 127 and 185 GPa, respectively. The compressive and flexural strengths at room temperatures are 475 and 350 MPa respectively. The thermal conductivity and the electrical resistivity at room temperature are found to be 12 W m^{-1} K^{-1} and 2.61x10$^6\Omega^{-1}$Vm^{-1} respectively. The temperature dependence of the electrical resistivity is typical of

metallic conductors. Like a metal, it is machinable, thermal-shock resistant, damage tolerant, relatively soft, and is both a good electrical and thermal conductor. Like a ceramic, it is elastically stiff, lightweight, has a low thermal-expansion coefficient, and maintains its strength to relatively high temperatures [71]. Polycrystalline samples of Ti_4AlN_3 fail in a semi-brittle manner at room temperature, but eform plastically at temperatures greater than 1000 °C. The compressive stress at which inelastic deformation is detected is 450 MPa. [42],[71]. The resistance of Ti_4AN_3 is high because of residual resistivity property, which likely reflects the fact that its actual chemistry is 4:1:2.9 rather than 4:1:3 [72],[73].

It has a hexagonal unit cell, with a space group $P6_3/mmc$ and lattice parameters $a = 2.9880\mathring{A}$ and $c = 2.3372\mathring{A}$ [74]. Initially, this ternary was believed to have a $Ti_3Al_2N_2$ chemistry and hexagonal structure. But recent results have shown that this compound was iso-structural with Ti_3SiC_2 [65], [58],[75],[76]. Thus various experimental results have conclusively shown that this compound is layered, wherein the layers of Al atoms are separated from each other by four layers of Ti. The nitrogen atoms occupy the octahedral sites between the Ti layers. The most important characteristic Ti_4AlN_3 shares with the other layered nitrides is the unique combination of high stiffness *(E > 300 GPa)* and ease of machinability. Like the others, Ti_4AlN_3 is machinable with regular high-speed tool steels, a bandsaw, or hacksaw, without lubrication or cooling required. At this time, the atomistic origin of this brittle-to-plastic transformation is unclear, but is believed to result from an enhancement in the ease

of grain rotation, grain deformation, delamination, and grain buckling. $Ti_4AlN_{2.9}$ is quite comparable to stoichiometric TiC. Rietveld analysis of neutron diffraction data indicate that the Al atoms in $Ti_4AlN_{2.9}$ vibrate significantly at higher amplitudes than the other atoms in the structure. Experimental results shows that the value of its conductivity is marginal between metallic and semiconducting leading to the suspicion of the presence of a small bandgap. The residual resistivity or resistance of $Ti_4AlN_{2.9}$ is higher than either Ti_3SiC_2 or $Ti_3Al_{1.1}C_{1.8}$. This difference is because of the scattering of the holes by the N vacancies present in $Ti_3AlN_{2.9}$ [42].The thermal expansions of Ti_4AlN_3 along the *a*- and *c*- axes are 9.6 and 8.8 x10^{-6} C^{-1}, respectively *(the expansion along the c- axis is shorter than along the a- axis).* This implies that the average bond strength along the *c*- axis, *(the direction that includes the Ti -Al bonds)*, is higher than along the *a*- axis. The thermal-expansion anisotropy is quite mild. This is surprising given the marked anisotropy in its mechanical properties, it is typical of the $M_{n+1}AX_n$ phases [74],[76].

$Ti_4AlN_{2.9}$ is the least conductive, not because of concentration, (it has a higher density of states at the Fermi Level), but due to low mobility of carriers, presumably due to scattering by vacancies. At low temperatures vacancies in non-stoichiometric transition metal nitrides are potent scatterers of electrons and they are quite comparable to stoichiometric TiC. Experimental results show that the value of its conductivity is marginal between metallic and semiconducting leading to the suspicion of the presence of a small gap. The residual resistivity or resistance is because of the scattering

of the holes by the N vacancies present in $Ti_4AlN_{2.9}$ [42],[58],[73]. It has been established that the oxidation behavior of Ti-Al intermetallics is strongly dependent on the aluminium content. Oxidation of $Ti_4AlN_{2.9}$ results in a striated microstructure. The oxidation of $Ti_4AlN_{2.9}$ which is a layer from the two phase mixture of TiN_x and Al, is the dissociation of $Ti_4AlN_{2.9}$ according to

$$Ti_4AlN_{2.9} \rightarrow 4TiN_{0.72} + Al \tag{4.5}$$

The oxidation then presumably proceeds by the oxidation of the Al and TiN_x, separately. The $M_{n+1}AXn$ phases do not melt, but slowly decompose into the MX_n compound and the A group element. The decomposition temperature is a function of impurities. It is apparent that $Ti_4AlN_{2.9}$ is less oxidation resistant which is not as good as the 211 phases. $Ti_4AlN_{2.9}$ decomposed in air at 1000°C into Al and the TiN_x just below the oxide layers that form. This decomposition, which occurs topotactically, does not affect the final morphology or the sequence of the layer that form, but slightly affects kx values, especially for $Ti_4AlN_{2.9}$ [72]. The decomposition temperature is a function of impurities. One of Ti_4AlN_3's greatest property is the ability to be used to avoid solar heating and also increase the radioactive cooling due to the increased thermal emittance compared to TiN. Therefore it can be regarded as a candidate for a coating material for temperature control of space vehicles.

Table 4.1: The lattice parameters of crystal structures of various hexagonal and cubic Ti-Al-N compounds.

Phase	Space Group	Calculated(Å)	Experiment(Å)
Al	$Fm-3m(225)$	3.978(3.999)	4.0497[79]
Ti	$Fm-3m(225)$	3.999(4.123)	4.06[80]
AlN	$F43m(216)$	4.344(4.400)	4.365[81]
TiN	$Fm-3m(225)$	4.178(4.251)	4.239[82]
Ti_2AlN	$P6_3/mmc$	a= 2.550(2.994), c= 13.421(13.402)	a= 2.994, c=13.61 [29]
Ti_3AlN	$Pm3m$	a= 4.055(4.129)	4.112[77]
$TiAlN_2$	$P6_3mc$	a= 4.166(4.235)	a= 3.962[78]
Ti_4AlN_3	$P6_3mc$	a= 2.546(2.444) c= 23.082(23.077)	a= 2.991 c= 23.396[74]

4.2 RESULTS AND DISCUSSION

4.2.1 Crystal Structure

For the Ti-Al-N system we considered the hexagonal structures of Ti_2AlN and Ti_4AlN_3 and the two cubic phases Ti_3AlN and $TiAlN_2$. Both though different represented the low and high N concentration structures [29],[77],[78],[74]. The crystal structure of the phases is shown in figure (4.2). For $TiAlN_2$ phase the cubic structure corresponded to Ti or Al occupying sites with equal probability and this showed the ability to be randomly distributed over the lattice. For the 8 *atom* unit cell displayed in the structures below, it was noted that a very small tetragonal distortion of $\sim 0.1\mathring{A}$ was present in the final calculated structure. This led us to consider two ways to obtain the elastic constants calculations. Firstly by treating the cell as if it were exactly cubic and by considering the tetragonal symmetry. There wasn't much difference in the results to the approaches that were implemented.

Table (4.1) shows the calculated results for the crystal structure for both LDA and GGA in brackets and the experimental values. There is a small percentage difference between the calculated results and the experimental results which shows the high accuracy of the computational calculations. For these calculations we have chosen to use the LDA to obtain the elastic constants. GGA was better used for the cell geometry as it underestimates elastic properties. It is emphasized that the purpose of the present work was to examine trends, although in the case of the stability of the phases both LDA and GGA formalisms were applied.

4.2.2 Relative Stabilities

For the stabilities only those of the Ti -Al - N system were considered. We looked at the enthalpies of the component atoms using :

$$\Delta E = E_{tot}(Ti_xAl_yN_z) - x\mu_{Ti} - y\mu_{Al} - z\mu_N$$

and the calculated total energy values where we were able to get μ_i (*atomic enthalpies per atom depending upon the stoichiometric composition*) to where ΔE is the formation energy, E_{tot}, the total energy $\mu_{TixAlyNz}$ the chemical potentials of the related atoms, x, y, z representing the number of atoms. The metal enthalpies can be directly obtained from a calculation on an appropriate metal structure *(usually cubic)*. However the nitrogen (N) enthalpy was difficult to estimate and for this reason

we considered two explicit situations. The first value was appropriate to the reaction:

$$\mu_N(1) = 2\mu_{TiN} - \mu_{Ti}$$

and the second

$$\mu_N(2) = 2\mu_{AlN} - \mu_{Ti}$$

There was quite a large difference between these values with $\mu_N(1) - \mu_N(2) \sim 1\text{eV}$ and that implied that the choice of phase formed critically depended on synthesis conditions. Thus we defined two formation energies essentially relating to the relative importance of TiN or AlN and these were:

$$\Delta E_1 = E_{tot}(Ti_xAl_yN_z) - x\mu_{Ti} - y\mu_{Al} - z\mu_N(1)$$

and

$$\Delta E_2 = E_{tot}(Ti_xAl_yN_z) - x\mu_{Ti} - y\mu_{Al} - z\mu_N(2)$$

Values for μ_N the formation energies are shown in Figure (4.1) [3] and the rich Ti structures are preferred especially where the concentration of Ti is greater than the concentration of Al *(i.e. Ti rich)* In the case of the ternary systems Ti_2AlN and Ti_4AlN_3 that would satisfy the relation that suggest $\Delta E(Ti_2AlN)/\Delta E(Ti_4AlN_3) = 0.5$.

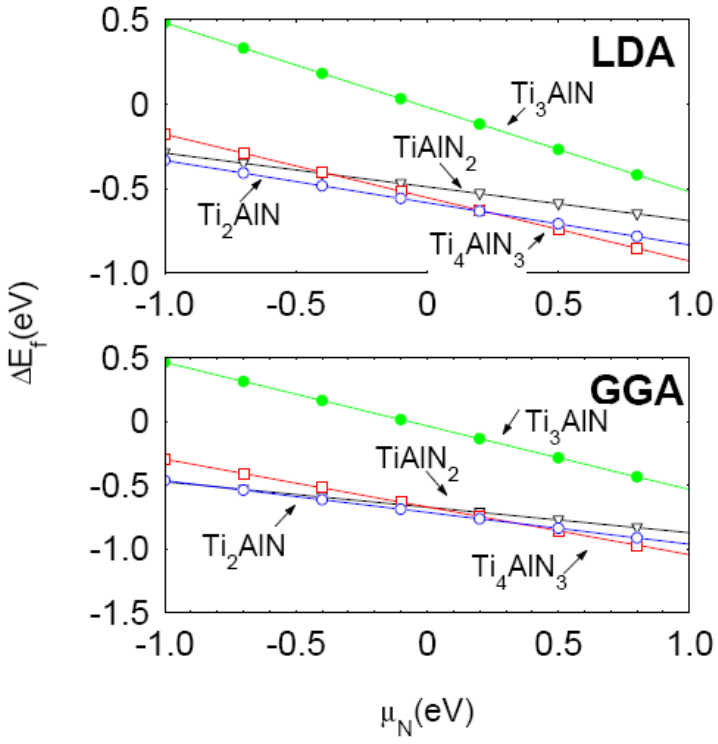

Figure 4.1: Stabilization energies for different nitrogen enthalpy; the zero is taken at $\nabla\mu_N = 0$ for AlN; $\nabla\mu_N > 0$ is for TiN.

Table 4.2: Total energies (eV/atom) of various Ti-Al-N phases using LDA, the GGA values are in brackets

Phase	B(GPa)	B′	E(eV/atom)	ΔE_1(eV)	ΔE_2(eV)
Al	85(77)	5.06(4.96)	-4.167(-3.764)		
Ti	123(112)	3.32(3.79)	-8.493(-7.763)		
AlN	211(175)	3.91(5.91)	-8.190(-7.4223)		
TiN	321(278)	4.39(4.12)	-8.924(-8.138)		
Ti_3SiC_2	207(183)	4.34(4.38)	-9.57(-8.75)		
Ti_2AlN	173(144)	4.39(4.12)	-8.924(-8.138)	-0.583(-0.716)	-0.348
Ti_3AlN	185(162)	4.17(4.16)	-8.861(-8.097)	-0.488(-0.675)	
$TiAlN_2$	290(256)	4.18(4.22)	-9.289(-9.292)	-0.018(-0.004)	0.050
Ti_4AlN_3	223(198)	4.52(4.29)	-9.902(-9.009)	-0.554(-0.710)	-0.202

4.2.3 Elastic Properties

Elastic properties of the various structures were obtained directly from the optimized cell structures using Energy/displacement method. From these values the general expressions was used to obtain the effective isotropic Bulk, Shear and Young moduli as well as Poisson ratio. The equation are stated below

$$B = \frac{1}{9}(c_{11} + c_{22} + c_{33} + 2(c_{12} + c_{13} + c_{23}))$$

$$G = \frac{1}{15}(c_{11} + c_{22} + c_{33} + 3(c_{44} + c_{55} + c_{66}) - c_{12} - c_{13} - c_{23})$$

$$E = \frac{9BG}{3B + G}; \qquad \nu = \frac{(3B - 2G)}{2(3B + G)}$$

Table (4.2) shows the two formation energies $\Delta E_1$and ΔE_2 relating to the rel-

ative importance of TiN or AlN as these two are the major constituents of the Ti- Al - N system. For Ti_2AlN we employed two approaches as we have generated the cubic and the hexagonal structure. The results shown in Table (4.2) are $\Delta E(Ti_2AlN)/\Delta E(Ti_4AlN_3) = 1.05$ and not consistent with Barsoum's suggestion. Therefore the simple concept of relating properties of Ti-Al-N phases directly to those of TiN we found not to be applicable. In other words our results have shown that the simple way of relating the formation enthalpy of the ternary Ti-Al-N structures to that of Ti-N as has recently been suggested in not applicable for the Ti-Al-N nitrides. We considered two approaches to calculate the various properties of Ti_2AlN, as a result we were able to have two stuructures, the cubic and hexagonal structures as shown in figures (4.2) and (4.3). However, the ab-initio computational calculations do show that many ternary nitrides in the Ti -Al -N system with different stoichiometries results in various different structures that are stable, but the formation of these structures depend on the nature of the component phase. Here we have considered three distinct systems and from this it is implied that the Ti_4AlN_3 is the hardest structure - as it has largest bulk, shear and Young moduli. We suggest that for this system the elastic moduli - bulk, shear and Young are also not directly related to the concentration of TiN but rather to the relative concentration of N and Ti depending on the relative enthalpies used.

Table (4.4) shows the bulk, shear and Young's moduli results that have been obtained from the elastic constants calculations in table (4.3).

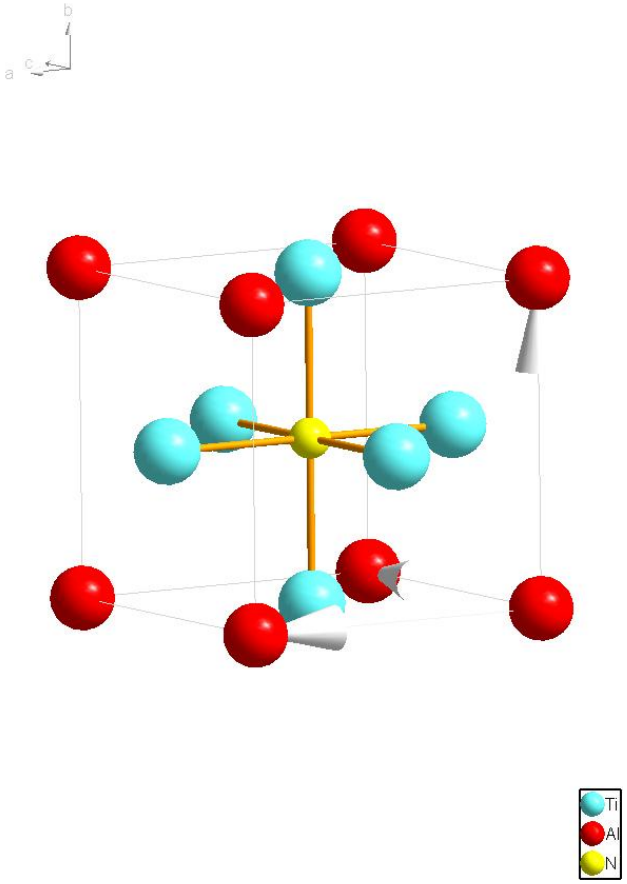

Figure 4.2: Cubic structure of Ti_2AlN (211)

Table 4.3: Calculated elastic properties using LDA from elastic constants from the De Beers Group

Phase	$\frac{[N]}{[Ti]}$	$\frac{[N]}{[Al]}$	c_{11}	c_{12}	c_{13}	c_{33}	c_{44}	c_{66}
Ti_2AlN	0.50	1.00	337	87	105	120	207	-
prev.cal. [51]			342	56	96	123	283	
Ti_3AlN	0.33	1.00	288	144	-	-	66	
Ti_3AlN_2(cubic)	2.00	2.00	573	155	-	-	200	
$TiAlN_2$(tetragonal*)			472	132	104	564	233	211
Ti_4AlN_3	0.75	3.00	454	117	112	172	438	
prev. calc.[51]			420	56	70	123	380	
expt.[78]								

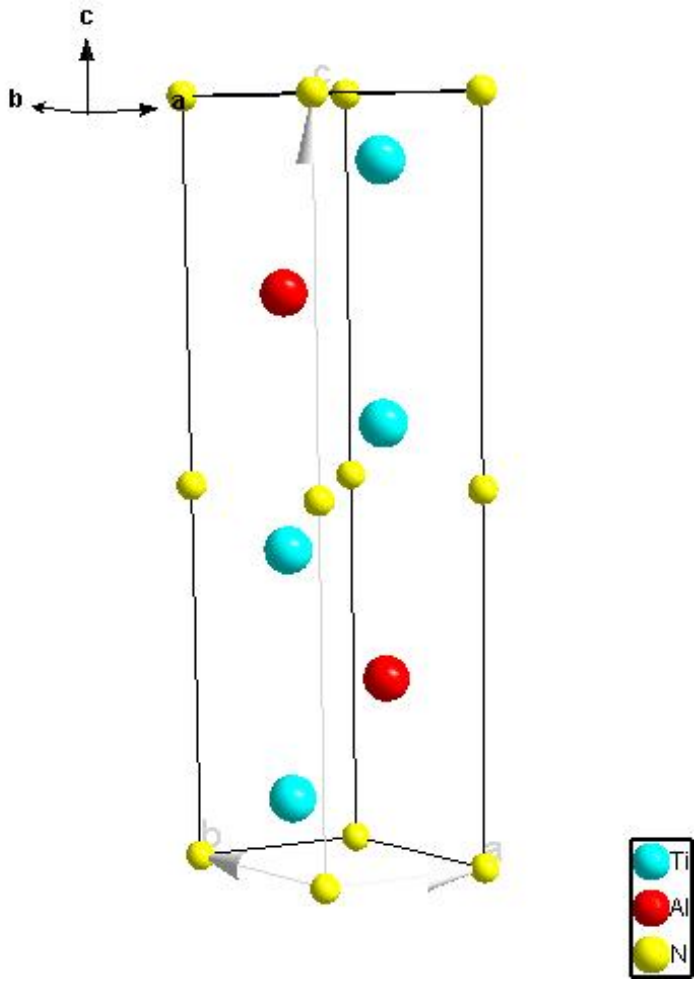

Figure 4.3: Hexagonal structure of $Ti_2AlN(211)$

Table 4.4: Calculated bulk, shear and Young moduli from the elastic constants from Debeers

Phase	B(GPa)	G(GPa)	Y(GPa)	υ
Ti_2AlN	174	109	273	0.24
previous calc.[51]	163	122	293	0.20
Ti_3AlN	192	68	183	0.34
Ti_3AlN_2(cubic)	295	203	496	0.22
$TiAlN_2$(tetragonal*)[51]	244	213	495	0.16
Ti_4AlN_3	255	135	339	0.25
previous. calc.	183	144	342	0.19
expt.[78]	185	127	310	0.22

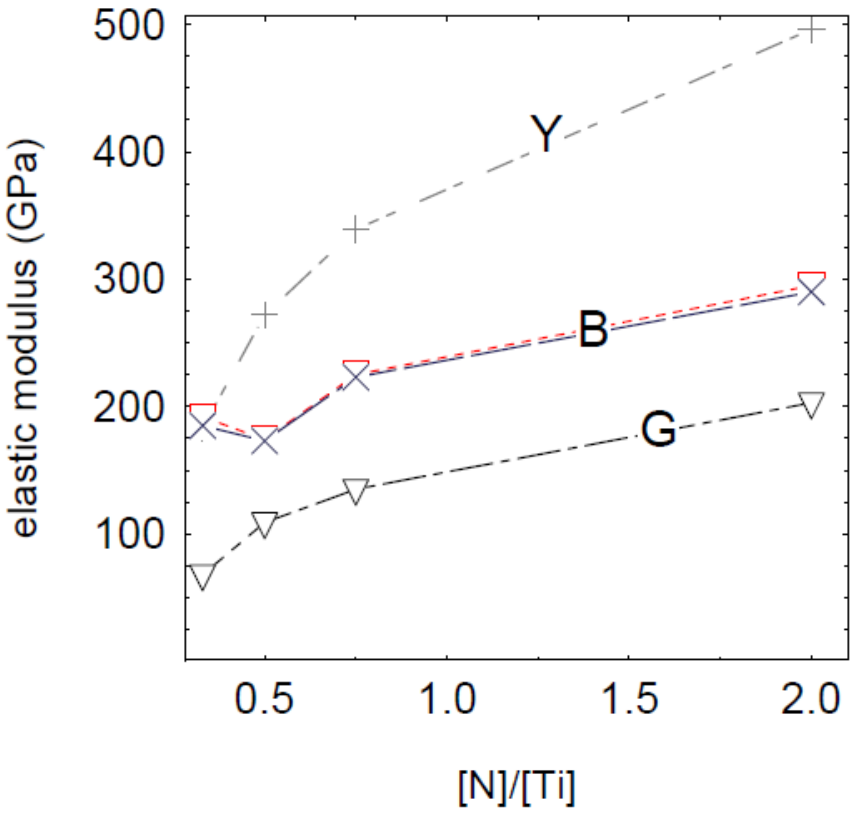

Figure 4.4: Calculated variation of elastic modulus with N: Ti modulus [3]

An estimate of using this approximation is seen when comparing the two calculations of elastic constants of the cubic and tetragonal systems. For a cubic system c_{33}=c_{11}, c_{12}= c_{13} and c_{44}=c_{66} and the results are shown in table (4.3), [51]. There is very little departure from this and the calculated effective isotropic elastic moduli are nearly the same. More important the trend relative to the other phases considered here is also shown.

An estimate of using this approximation is seen when comparison. In Figure (4.4)

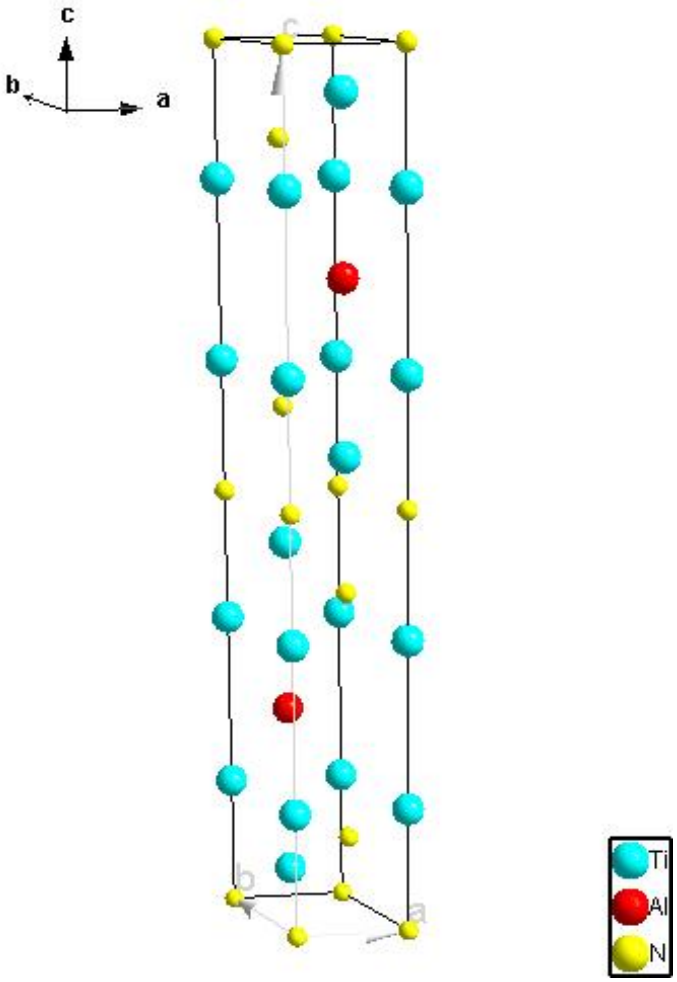

Figure 4.5: Hexagonal structurer of Ti_4AlN_3(413)

we show the expected variation in the various moduli for different N concentrations relative to Ti.

4.2.4 Other electronic structures

Ti_4SiC_3 shown in figure (3.2) below has been found to be "mirror" image of Ti_3SiC_2 figure (3.3) and figure (3.3) has been found to be iso-structural with Ti_4AlN_3 (figure

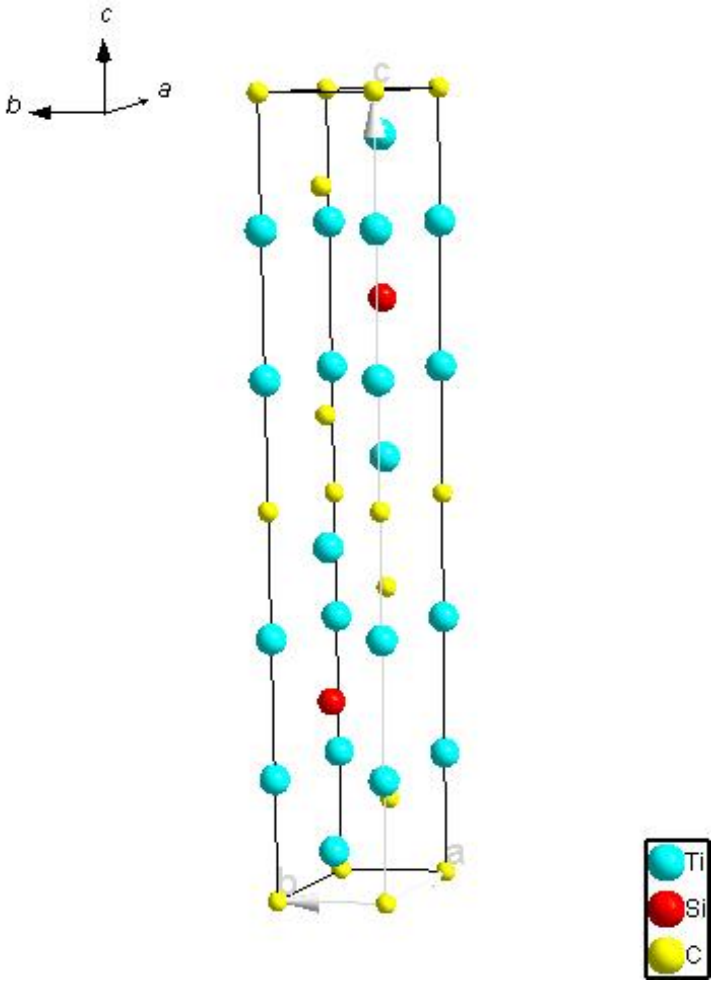

Figure 4.6: Hexagonal structure of Ti_4SiC_3(413)

(4.5)) above. Since both Ti_4SiC_3 and Ti_4AlN_3 belong to the 413 max phase their atomic structure arrangement is similar. It could be that they have more similarities not only in atom arrangement but also in some of their application properties. This might be possible even though one belongs to carbides and the other to nitrides.

Figure (4.7) is the electronic structure of Ti_3AlN, in its cubic form. This compound does fill the *B-type* crystal structure described earlier.

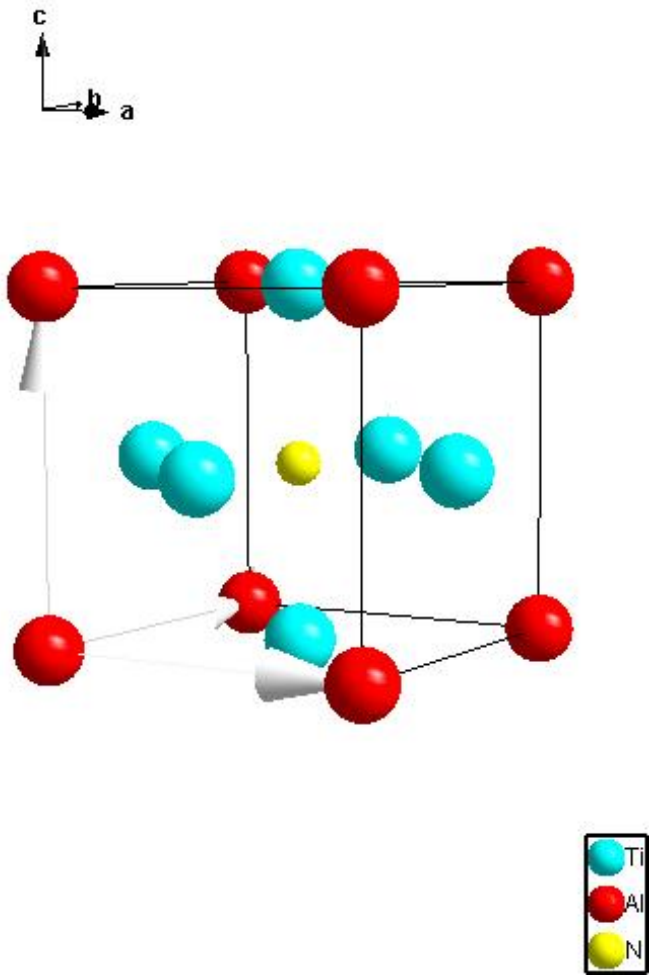

Figure 4.7: Cubic structure of $Ti_3AlN(311)$

Chapter 5

Conclusion

The search for new materials is still on going with new discoveries being done experimentally and theoretically on new groups of materials. MAX phases are no exception to these discoveries. In this work we have paid attention to the max phases belonging to both the Ti – Si – C and Ti – Al - N systems. Ab – initio calculations using VASP code were carried out to determine the energy of states (EOS) bulk modulus, lattice constants and total volume of both the LDA and GGA .

For the Ti – Si –C max phase, the theoretical work done included not only the physical properties of these max phase 211, 321 and 413 groups, but we were able to carry out a comparison of Ti_3SiC_2 with a newly discovered phase Ti_4SiC_3 focusing on their electronic structures and density of states. These two have been found to be "mirror" images of each other. Our results on their electronic structures and density of states do concur with the theoretical work that has been previously done. Further

work to be done will be to investigate their elastic constants, charge densities and relative stabilities.

Furthermore we included the so called "fictitious" Zr_3SiC_2 phase, that has been found experimentally to exist as a means to display two – phases $Zr_5Si_3C_x$ and ZrC_{1-x}. Also Hf_3SiC_2 structure was included. The two phases (Zr_3SiC_2 and Hf_3SiC_2) showed similarities in their atom arrangement of their electronic structures and with Ti_3SiC_2. Results on their EOS bulk modulus were similar not only to each other, but also to Ti_3SiC_2. However, it was expected that their density of states would be similar to each other, but it was noticed that the density of states for Hf_3SiC_2 is more similar to Ti_3Sic2, than Zr_3SiC_2.

It can be assumed that maybe in the future Zr_3SiC_2 will be used instead of Ti_3SiC_2 as Ti and Zr both help to improve wetting of ceramic joint microstructures. For the Ti – Al – N max phase, our research not only included their electronic structures and EOS (energy of states) bulk modulus, but also the relative stabilities. We were able to conclude that for the formation energies TiN and AlN in this system are the major role players in the formation of these max phases and that rich Ti structures are preferred especially where the concentration of Ti is greater than the concentration of Al. Also relating properties of Ti-Al-N phases directly to those of TiN are not applicable, this means relating the formation enthalpy of the Ti-Al-N structures to that of Ti- N does not apply to these nitrides. Future work could be done on the possible defects of both the Ti-Si-C and Ti – Al –N max phase and their charge

densities and more structures.

Bibliography

[1] M. W. Barsoum, *et al.*, *A Metallurgical and Materials Transactions* **33A**, 2775 (2002).

[2] R. Ahuja, O.Eriksson, J. M. Willis, B.Johansson, *Applied Physics Letters* **76**, 2226 (2002).

[3] D. B. R. Group.

[4] K.Iakouboviskii, G.J.Adrianenssens, *Physical Review B* **62**, 16587 (2000).

[5] C. Science, T. News, *www.caltechnews.com* (2007).

[6] J. D. Hettinger, *et al.*, *Physical Review B* **72** (2005).

[7] L. Chaput, G. Hug, P. Pecheur, H. Scherrer, *Physical Review B* **75** (2007).

[8] H. Hogberg, *et al.*, *Surface and Coatings Technology* **193**, 6 (2005).

[9] M. M. M.D.Graef, *Structure of Materials: An Introduction to Crystallography Diffraction Symmetry* (Cambridge : Cambridge University Press, 2007).

[10] J. A. Warmer, S. K. R. Patil, S. V. Khare, K. C. Masiulaniec, *Applied Physics Letter* **88**, 101911 (2006).

[11] M.W.Barsoum, T.Zhen, S.R.Kalidindi, M.Radovic, A.Murugaiah, *Natural Materials* **2**, 107 (2003).

[12] B.Holm, R. Ahija, S. Li, B.Johansson, *Journal of Applied Physics* **91**, 9874 (2002).

[13] D.Joubert, *Lecture Notes in Physics* **500**, 47 (1997).

[14] R. G. Parr, W. Yang, *International Series of monographys on Chemistry* **16**, 152 (1989).

[15] K.Capelle, *http://arXiv.org/archive/cond - mat* **4**, 3 (2005).

[16] R.M.Martin, *Electron Structure: Basic Theory and Practical Methods* (Cambridge Press, 2004).

[17] L. D.J.Singh, *Condensed Matter Sciences Division* pp. 6–13 (1962).

[18] J. P. Perdew, K. Burke, M. Ernzerhof, *Physical Review Letters* **77**, 3865 (1996).

[19] C. Kittel, *Introduction to Solid State Physics* (John Wioley and Sons, 1996), 7th edn.

[20] H.J.Monkhorst, J.D.Pack, *Physics Review B* **13**, 5188 (1976).

[21] D. R. Harmann, M. Schluter, C. Chiang, *Physical Review Letters* **43**, 1494 (1979).

[22] G. Kresse, J. Hafner, *Journal of physics: Condensed Matter* **6**, 8245 (1994).

[23] W.A.Harrison, *Electronic Structure and the Properties of Solids : The Physics* (San Francisco : Freeman, 1980).

[24] G.Kresse, D.Joubert, *Physics Review B* **59**, 1758 (2001).

[25] G.Kresse, D.P.Jourbet, *Physical Review B* **59**, 1758 (1999).

[26] P.E.Blochl, *Physical Review B* **50**, 17953 (1994).

[27] Y. Wang, A. H. Carim, *Journal of America Society* **78**, 662 (1995).

[28] P. Riley, E. H. Kisi, T. C.Hansen, A. W. Hewat, *Chemistry and Structure* (2001). Annual Report.

[29] H. W.Jeistscho, F.Benesovysky, *Monatshefte fuer Chemie* **94**, 1198 (1963).

[30] J.Wang, Y. Zhou, T. Liao, J.Zhang, Z.Lin, *Acta Materialia Inc.* **58**, 227 (2008).

[31] P.Finkel, M.W.Barsoum, T. Raghy, *Journal of Applied physics* **87** (2000).

[32] B.J.Kooi, R.J.Popper, N. Carvallo, J. Hosson, M.W.Barsoum, *Acta Materialia* **51**, 2859 (2003).

[33] El-Raghy, M. Barsoum, *Journal of American Ceramics* **10**, 2849 (1990).

[34] H.Klemm, K.Tanihata, T. Abe, *Journal of Material Science* **28**, 1557 (1993).

[35] G. T. W.Gulbinski, A., W.Warcholinski, *Surface Coatings Technology* **180 - 181**, 341 (2004).

[36] W. Wakelkamp, F. V. Loo, R.Metselaar, *Journal of the European Ceramic Society* **8**, 135 (1991).

[37] R. J.Lis, Y.Miyamoto, K.Tanihata, *Materials Letter* **22**, 163 (1995).

[38] J. L. J.Lis, R.Pampuch, *Ceramic International* **19**, 219 (1993).

[39] Z.J.Lin, M.J.Zhuo, Y.C.Zhou, M.S.Li, J.Y.Wang, *Scripta Materialia* **55**, 445 (2006).

[40] T.El-Raghy, A. Zavaliangos, M. W. Barsoum, S. R. Kalidindi, *Journal of American Ceramics Society* **80**, 513 (1997).

[41] N. I. Medvedeva, D. L. Novikov, A. L. Ivanovsky, M. V. Kuznetsov, A. J. Freeman, *Physical Review B* **58**, 16043 (1998).

[42] T. P. of Ti4 Al N3, *Journal of Applied Physics* **87**.

[43] S.Li, R.Ahuja, M.W.Barsoum, P.Jena, B.Johansson, *Applied Physics Letters* **92** (2008).

[44] H.I.Yoo, M.W.Barsoum, T.El-Raghy (2000).

[45] J.L.Jordan, *et al.*, *Journal of applied Physics* **93**, 9639 (2003).

[46] H. Hogber, *et al.*, *Surface and Coatings Technology* **193**, 6 (2005).

[47] . C. M. Fang, Et. al, *Physical Review B* **74**, 0541061 (2006).

[48] M.Magnuson, *et al.*, *Physics Review B* **76** (2007).

[49] A. U. Erigashin, A. L. Ivanovskii, *Theoretical and experimental chemitry* **45**, 98 (2009).

[50] D. R. Z.Sun, J.Zhou, J. Schneir, *Scripta Materials* **54**, 105 (2006).

[51] B. B.Holm, R Ahuja, *Applied Physics Letters* **79**, 1450 (2001).

[52] L. H. R.Yu, X.F.Zhang, Topology of charge density and elastic properties of Ti3SiC2 polymorphs, Ph.D. thesis, Materials Science Division, Lawrence Berkely National Laboratory , Berkely, CA 94720 (2004).

[53] G.Hug, E.Fries, *Physical Review B* **65**, 65 (2002).

[54] M.Magnuson, *et al.*, *Physical Review B* **74**, 205102 (2006).

[55] M.W.Barsoum, *et al.*, *Journal of American Ceramic Society* **82**, 2545 (1999).

[56] G.Chen, B.Sundman, *Journal of Phase Equilibria* **19** (1998).

[57] J. Schuster, J. Bauer, *Journal of Solid State Cemistry* **53**, 260 (1994).

[58] L.Farber, M.W.Barsoum, T. Raghy, T.Tzenov, *Journal of Applied Physics* **86** (1999).

[59] D.Vogtenhuberpawelczak, P.Herzig, J.Klima, *Zeitschrift Fur Physik B - Condensed Matter* **84**, 211 (1991).

[60] P.H.Mayrhfer, D.Music, J.M.Schneider, *Applied Physics Letters* **88**, 071922 (2006).

[61] V.Dolique, *et al.*, *Journal of Applied Physics* **103**, 083527 .

[62] M.Y.Gamarnik, M.W.Barsoum, T. E. Raghy, *Powder Diffraction* **15**, 241 (2000).

[63] Y. Zhou, Z. Sun, *Physical Review B* **61**, 12570 (2000 - 1).

[64] H.Faraoum, R.Terki, C.Esling, H.Aourag, *Materials Science and Engineering B - Solid State Materials for Advanced Technology* **110**, 280 (2004).

[65] V.Raghavan, *Journal of Phase Equilibria and Diffusion* **27** (2006).

[66] T.Liao, J.Wang, Y.Zhou, *Journal of Physics Condensed Matter* **18**, 6183 (2006).

[67] Y.S.Han, K.B.Kamykov, S.F.Dunaev, A.I.Zaitsev, *Journal of Phase Equilibria and Diffusion* **25**, 427 (2004).

[68] J.Magnan, G.C.Weatherly, M.C.Cheynet, *Metallurgical and Materials Transactions - a- Physical Metallurgy and Materials Science* **30**, 19 .

[69] A.T.Procopio, T. Raghy, M. .Barsoum, *Metallurgical and Materials Transaction* **31A**, 373 (2000).

[70] H. D. Lee, W. Petuskey, *Journal Of American Ceramic Society* **80**, 604 (1997).

[71] A.T.Procopio, M.W.Barsoum, T.El-Raghy, *Metallurgical and Materials Transations* **31A**, 333 (2000).

[72] M.W.Barsoum, N.Tzenov, A.Procopia, T. Raghy, M.Ali, *Journal of the Electrochemical Society* **148**, c551 (2001).

[73] P.Finkel, M. A. .W.Barsoum, J.D.Hettinger, S.E.Lofland, H.I.Yoo, *The American Physics Society* **67**, 235108 (2003).

[74] C.J.Rawn, *et al.*, *Materials Research Bulletin* pp. 1785 – 1796 (2000).

[75] D.Music, R.Ahuja, J.M.Schneider, *Applied Physics Letters* **86** (2005).

[76] A.T.Procopio, M.W.Barsoum, T.El-Raghy, *Physical Metallurgy and Materials Science* **31**, 333 (2000).

[77] J. J.S.Schuster, *Journal of solid state chemistry* **53**, 260 (1964).

[78] K. S.Inamura, F.Kanamura, *Journal of solid state chemistry* **68**, 124 (1987).

[79] A.J.Cooper, *Acta Crystallographica* **1**, 578 (1962).

[80] G. J.Haglund, F.Fernandez Guillermet, M.Korling, *Physical Review B, Condensed Matter* **48**, 11685 (1993).

[81] S. C.Yeh, Z.W.Lu, A.Zunger, *Physical Review B* **46**, 10086 (1992).

[82] A. Christensen, *Acta Chemica Scandinavica, Series A* **89**, 32 (1978).